CHAPTER 4

STRUCTURAL GEOLOGY

4.1. GENERAL

Structural complexity of the Lunavada-Santrampur area is very obvious from the geological map of the region (Fig. 3.2) and especially by the shapes and trends of quartzite ridges and hills as seen on 1: 50,000 Survey of India toposheets and satellite imagery (Fig. 3.1). The information obtained from these sources has been supported by detailed mapping of selected crucial areas. Fig. 4.1 is the structural map of the area prepared by the author. The present study has enabled the author to unravel the complexities of the deformational history of the area and the sequence of superposed foldings. It has been possible for him to work out a succession of at least three fold events. His analysis of the structural elements have led him to understand the interference of these folds in different combinations which have provided a rather fascinating diversity of outcrop patterns. A critical examination of the outcrop patterns in different parts of the study area supported by domain-wise structural analysis with the help of Schmidt Equal Area Stereographic Net has not only led to establishment of the sequence of fold events but has also elucidated the response of linear and planar structures (fold axes, axial planes and bedding planes) to the successive fold episodes. good

It will be seen from the description incorporated in the following pages of this chapter that the diversity in the orientation and behaviour of the fold events has been

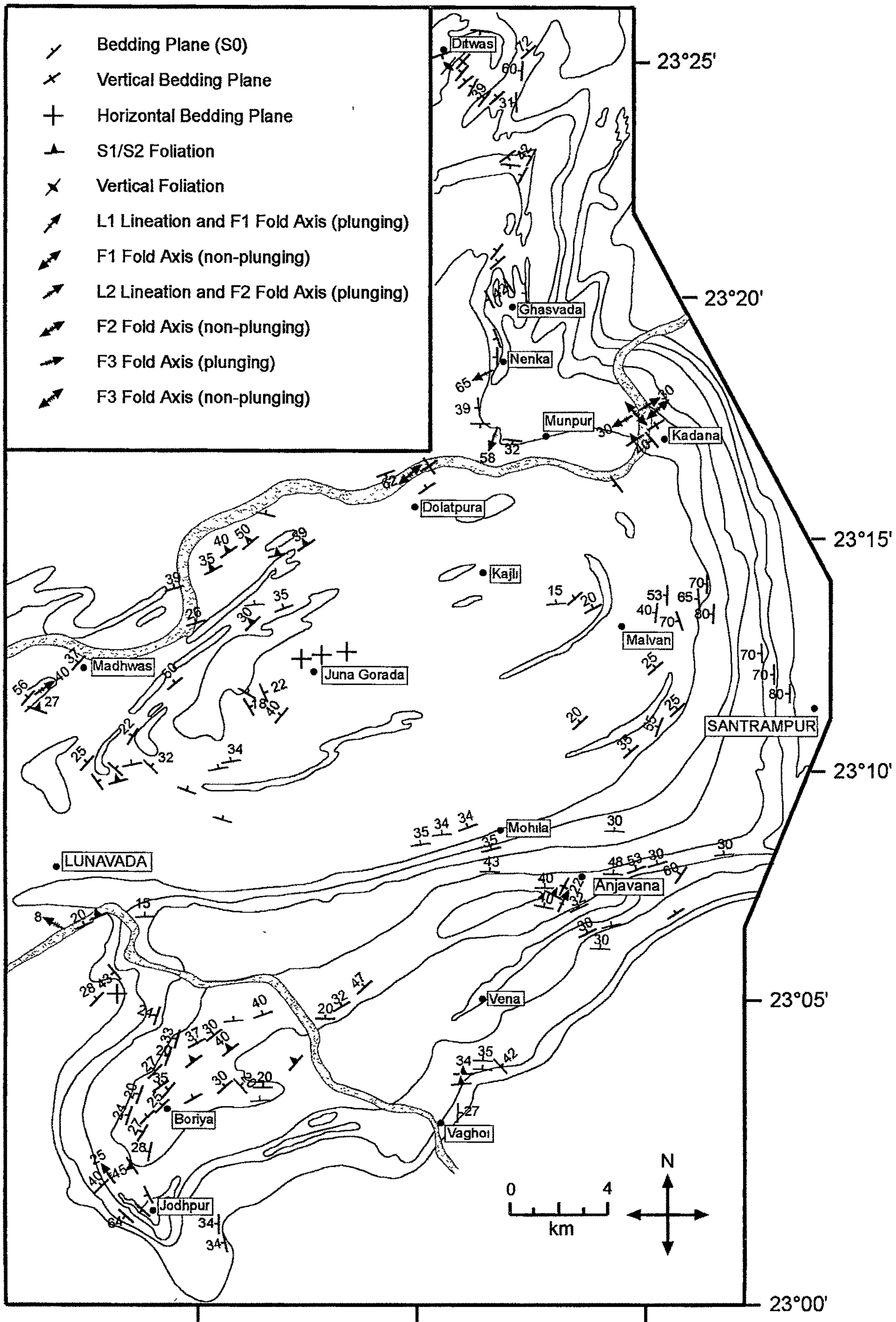

Fig.4.1. Structural Map of the study area.

controlled by mainly two factors. Firstly, the original trends of the different fold events were variable in different parts of the area. Secondly, the variation in the orientation of the surfaces on which the folds were superimposed controlled the behaviour of the superposed folds.

The structural history of the study area can be summarized by invoking a succession of three main fold events - F_1, F_2 and F_3 such that F_1 and F_2 have been broadly coaxial with NE-SW trend and rather compressed and tight at many places. At a few places variable trends for F_1 and F_2 have been recorded. The F_3 folds are NW-SE trending cross folds and these have developed as open flexures on regional scale limbs of F_1-F_2 folds (Mamtani, et al., 1998). By and large, the regional outcrop pattern is mainly due to the interference of F_1-F_2 with F_3 and the resulting oval distorted shapes on regional scale are due to this cross folding. The interference of F_1 and F_2 is observed as refolded folds ideally seen regionally in the outcropping quartzite ridges.

4.2. REGIONAL STRUCTURAL FRAMEWORK

As explained in chapter 3, for the purposes of structural description, the study area has been divided into three sub-regions, each characterized by its own interference pattern. Detailed structural analysis have enabled the author to more or less precisely recognize the different fold events present in various parts of the area and to work out the orientations of fold axis of the three fold episodes. Description of structures preserved in the three sub-regions is given below. Repeated

4.2.1. Sub-region I : Area to the north of Kadana-Dolatpura line (i.e. north of Mahi river)

The rocks to the North of Mahi river falling within the study area are observed to indicate dominant effects of first two foldings F_1 and F_2 both being coaxial to one another. This fact is obvious from the shapes and trends of the quartzite ridges. The outcropping ridges are made up of tight macroscopic F_1 folds over which F_2 folds have been superimposed. Whereas the trends of the axial plane of F_1 follow the trends of the ridges, the F_2 folds are somewhat open and show axial planes trending broadly due NE-SW. These observations have been supported by the satellite imagery studies (Fig.3.1) and substantiated by the stereographic analysis of the planar structures recorded during mapping. The area does not show many mesoscopic scale folds. However, the satellite image of this sub-region and the terrain to its WSW (which does not come under the study area) provides valuable information, because here a large number of tight refolded folds are revealed by closely spaced quartzite-ridge lineaments. The trends of the quartzite ridges and the axial traces of the tight folds (obviously F_1 and F_2) show identical NE-SW direction. The image also shows very clearly the tight refolded pattern (Fig. 3.1). The author has observed the presence of an F_2 fold hinge in the quartzites at Munpur (Fig. 3.5). The axis of the fold shows a plunge of 58^0 due SW. Although, small-scale folds are scarce but useful information is obtained by recording the cleavage-bedding relationship (F_2) in the well sections (Fig. 3.3). Another significant structural feature is the abundant NE-SW trending fracture cleavage which coincides with the axial plane of the mesoscopic F_2 folds. These fractures are either vertical or dip steeply to the NW. Such oblique relationships between bedding plane and axial plane fractures are recorded in quartzites alternating with chlorite schists around Ditwas, Kesarpura and Kampa in the sub-region I. In Ditwas area, there is a variation in lithology and this has been of considerable use in identifying the bedding planes especially in well sections. The variation is in the amount of quartz content in chlorite schists with some beds being richer in quartz than the others. As a consequence, the two lithologies are well demarcated. The quartz poor layers are thinner and have a thickness of about 5 cm while the silica rich layers have a thickness of around 15 cm. Around Ditwas, the bedding planes have a general strike of NE-SW and vertical dips. The axial plane fractures and cleavage trend NE-SW and dip moderately due W. Around Kesarpura, 1.5 km S of Ditwas, the bedding planes strike NE-SW and dip gently to the W. The axial plane fractures here have a N-S trend and show moderate dips due W. Similarly, around Kampa which lies further S of Ditwas, the bedding planes have a N-S trend with gentle dips to the W. The axial plane fractures here strike NNE-SSW and dip steeply to the WNW. At this locality, the quartzites have developed axial plane fractures (fracture cleavage) while the intervening chlorite schists have developed axial plane foliation - both having identical orientation.

At Kadana, on the banks of the river Mahi, development of culminations and depressions is observed in quartzites (Fig. 3.4). This is on account of the superposition of F_3 over F_2 on the mesoscopic scale.

Although the exposures in this sub-region-I do not show development of recognisable F_1 folds, the presence of a well developed crenulation cleavage (on microscopic scale) in the chlorite schists around Ditwas area confirms that this region did undergo an episode of deformation prior to the F_2 folding; the S_1 schistosity related to F_1 folding is parallel to the bedding plane (S_0).

Thus, on the basis of topographic studies, field observations and satellite data the structure of this sub-region reveals two fold events more or less coaxial. Although no significant effect of NW-SE cross folding (F_3) is seen (except at Kadana) some variation in the F_2 axis trend as obtained from structural analysis (Section 4.3) can be attributed to F_3 folding.

4.2.2. Sub-region II : Area to the south of Mahi river upto the Lunavada-Santrampur tract

To this sub-region belong the rocks lying to the south of Mahi river upto the Lunavada-Santrampur line. The outcrop pattern of the quartzite ridges here are seen to form a somewhat distorted oval shaped or eye-shaped structure, obviously a product of cross folding involving F_1-F_2 and F_3. This outcrop can be categorized as a Type I Interference of Ramsay and Huber (1987), i.e. dome and basin interference which develops on account of cross folding. The quartzite ridges that show the oval or eye-shaped pattern enclose a depressed area which is occupied by mica schists. In this sub-region, the outcrop pattern of quartzite ridges and the satellite data clearly point to the effect of interference of all the three fold events F_1, F_2 and F_3. It is observed that bedding planes in the quartzites in the northern and southern parts dip gently in a northerly direction. Bedding planes along the eastern margin show a more or less N-S trend and steep dips due W. In the west, the area is marked by a macroscale fold closure. Here the quartzites of the N and S converge into a fold, the axis of which plunges gently due NE. Though F_2 folds are not observed on mesoscopic scale, this fact is well brought out by the stereographic analysis of field data (Section 4.3).

In Ankalva area, located close to the regional F_2 fold closure, good exposures exhibiting bedding and cleavage relationship (generally sub-parallel to each other) are encountered (Fig. 3.9). However, at a few localities they are slightly oblique to one another. A mesoscopic F_2 fold is observed in quartzite along a road cutting around Limbodhra (8 km N of Lunavada on the Lunavada-Modasa highway) with the fold axis plunging moderately to the NE (Fig. 3.8). Alternating chlorite schists and quartzite sequence is also observed around this area; the schistosity is sub-parallel to the bedding plane.

Mesoscopic F_2 folds of the order of several meters in the Dolatpura area have been recorded in the quartzites and chlorite schists (Fig. 3.7). These folds are of recumbent nature. A series of F_2 flexures in quartzites gives a step like appearance. The axial plane cleavage developed in the schists is sub-horizontal.

It is worth highlighting here that the F_2 axes in Ankalva area (SSW of Dolatpura) and falling within Sub-region II and in Munpur (NE of Dolatpura, falling in Sub-region I) have different orientations and directions of plunge. This variation in the attitudes of the F_2 fold axis has been found to be due to the superposition of F_3 folding on F_2 in this sub-region. This fact has been clearly brought out on the basis of structural analysis (section 4.3).

4.2.3. Sub-region III : Area to the south of Lunavada-Santrampur tract on the two sides of Panam river

The sub-region III comprising southernmost part of the study area shows a very complex outcrop pattern on account of the effect of all the three fold events - F_1,

F_2 and F_3 (Fig. 3.1, 3.2). Although, here also, the regional pattern on a cursory-look resembles a distorted closed structure, on a very careful scrutiny, the shape of the outcropping area is seen to be different from that of the Sub-region II. Here, the two limbs of a F_2 fold have been brought quite close to each other at the eastern end. The area is replete with numerous quartzite ridges following diverse orientations. Outcrop pattern and satellite image show presence of regional F_1 and F_2 folds. The distortion is due to the superimposition of F_3 folding. Macroscopic fold pattern resembles a distorted Type-III Interference of Ramsay and Huber (1987), i.e. convergent and divergent interference on account of superimposition of F_2 over F_1 followed by a distortion which is attributed to F_3 cross folding.

The rocks of this area show development of a few discrete mesoscopic folds some of them are easily identifiable while others have been established with the help of stereographic analysis of structural data recorded in the field.

Quartzite ridges in Sub-region III form limbs of F_1 and F_2 folds. On each F_2 limb, F_3 folds are superposed which has resulted in open flexuring of quartzite ridges with axial traces trending NW-SE to WNW-ESE. Such F_3 flexures are observed on macroscopic scale around Satatalav, Chandsar and Boriya areas, all lying to the south of Lunavada. As is revealed from structural analysis (Section 4.3), the direction of plunge of the F_3 fold axis in this Sub-region varies from NW to WNW. A clearly discernible macroscopic fold is recorded in Ratanpur-Vaghoi area (3 km S of Vena in Fig. 3.2) on the ENE-WSW trending quartzite at the southernmost extremity of this sub-region.

Presence of the nose of a large scale F_1 fold is observed at Kotha, SE of Lunavada. Although the actual fold is not observed on mesoscopic scale, the fold is well established on the basis of structural analysis, such that the F_1 fold axis is statistically recorded to plunge gently to the NE.

A number of F_1 reclined folds are present at Anjavana, 18 km ESE of Lunavada (Fig. 3.11 to 3.14). Folds developed in alternating quartzite-mica schist sequence here have a NE-SW trend and plunge gently to the NE. The microstructural studies of mica schists from the nose of the reclined folds reveal that they do not possess any crenulation cleavage, thus confirming that these folds are F_1 folds. A prominent mineral lineation plunging gently to the NNW is present on the foliation planes of these schists.

No mesoscopic F_2 folds are seen in this area. However, their presence on macroscopic scale is quite clear from the map pattern, structural mapping and analysis of structural data. Structural analysis of the area around Reganpaliya and Boriya, lying to the S of Lunavada shows that the F_2 fold axis here is plunges moderately to the NE. The F_2 axis in the southwestern extremity of the area which marks an F_2 fold closure has a plunge due NW. The variation in the direction of the F_2 axis is due to superimposition of the F_3 folds on F_2. It is interesting to note that the F_3 folds that have developed on the limbs of the F_2 folds in the above area also have a similar orientation as F_2.

Another interesting observation in this sub-region is the presence of kinks related to F_3 folding in schists occurring on the banks of the river Panam (S of Lunavada). The kink axis plunges very gently due WNW (Fig. 3.16).

4.3. STRUCTURAL ANALYSIS

A detailed analysis of the structural data using Schmidt Equal Area Stereographic Net has enabled the author to determine the nature and behaviour of folding in various parts of the study area. It may be repeated here that exposures of rocks are scarce in the area around Lunavada and Santrampur as a consequence of which there is paucity of available data on planar and linear structures. The scale of folding is regional with relatively scarce small scale linear and planar structures and this has made the direct determination of the structure of the area rather difficult. In such a situation, the stereographic analysis has proved a very useful tool to work out the orientations of successive fold events with the help of β and π diagrams.

During field work, the present author has recorded orientations of all measurable planar and linear structures. The most prominent planar structures which the author has recorded are the bedding planes (S_0 surfaces). Axial planes and lineations were recorded wherever preserved. This field data was plotted on the stereographic net to prepare β and π diagrams using the techniques described by Turner and Weiss (1963), Ramsay (1967) and Ramsay and Huber (1987). Considerable heterogeneity in structural elements is observed in the study area on account of (i) variation in lithology and (ii) superimposition of several deformations and (iii) variation in the intensity of deformation in different parts of the area.

Therefore, to analyze the structural data, the entire study area was divided into 12 *Structural Domains* (Domain I to XII; Fig. 4.2) - each domain possessing a near-homogenous deformational pattern. Domainal division of the area was done on the basis of (a) homogeneity and persistence of strike direction and (b) presence of macroscopic fold closures. Domains which have preserved several macro-fold closures within them were further sub-divided into different sub-domains for the purposes of analyzing each macro-fold individually. The planar features (S-surfaces) in each domain were plotted to get the β- intersection points and the total number of β-intersection points were determined by the formula n(n-1)/2, where n is the number of surfaces plotted. The β-diagram on contouring gave one or more maxima. This has helped in determining the effects of successive fold episodes on the orientation of S-surfaces and in deciphering the trends of various fold axes in a particular domain. Intersection of the limbs gave the β-axis i.e. fold axis using which the axial plane was determined. Similarly, the π-diagrams were prepared using the poles of the planes and the orientations of the limbs, π-axis (i.e. fold axis) and axial plane were determined for fold/s in each domain.

On account of effects of interference of three fold episodes, in several domains the contoured β-diagrams show more than one maxima. Obviously, these point to situations where these different maxima represent either axes of folds of different generations or they comprise different positions of F_1 and F_2 axes due to superposition of F_3 folding. Attempts were made to recognize and assign different

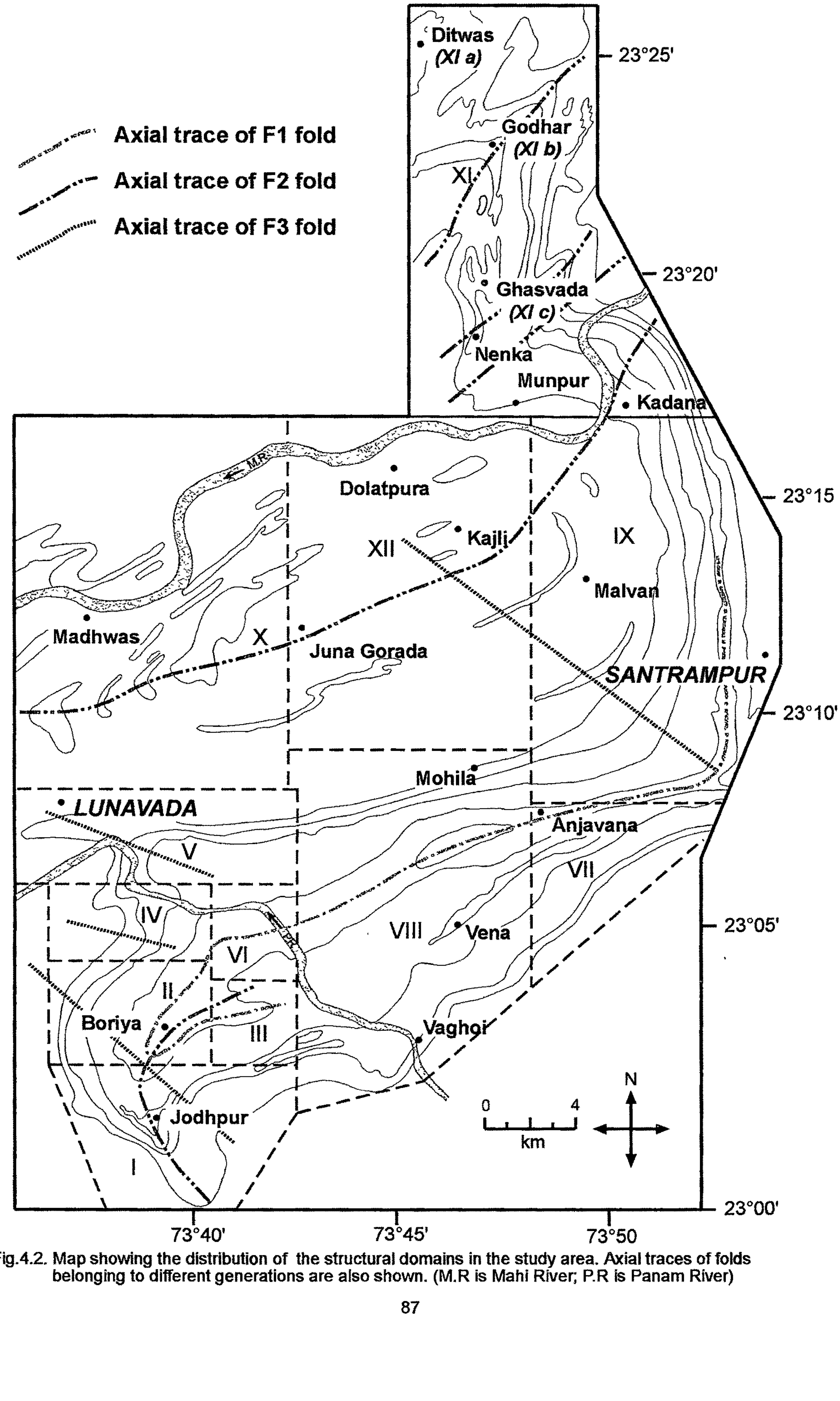

Fig.4.2. Map showing the distribution of the structural domains in the study area. Axial traces of folds belonging to different generations are also shown. (M.R is Mahi River; P.R is Panam River)

maxima to successive folds. For this maxima categorization of selected smaller areas within various domains showing clear presence of F_1 , F_2 and F_3 was done and accordingly relevant maxima (= fold axes) were recognized, and the comparable maxima on the main girdle were assigned to appropriate fold events. In trying to relate different maxima to one or other fold events in a particular domain, help was also taken of the data obtained from the adjoining or nearby domains. In some cases however, uncertainty has prevailed on account of scarcity of exposures and inadequate field data. Nevertheless, the integrated picture emerging out of the syntheses of information furnished by domainwise analysis has to a large extent enabled the author to arrive at a reasonably dependable structural pattern.

Domain I :

This domain comprises a macroscopic F_3 fold. Structural elements recorded on the mesoscopic scale are S_0, S_1 and S_2 all of which are virtually parallel to one another. Although there is paucity of structural (field) data from this domain because of the scarcity of field exposures, the β and π-diagrams provide information about the orientation of the fold axes (F_3) and the orientations of the macroscopic fold limbs (Fig. 4.3). The contoured π-diagram gives two maxima such that a great circle passes through them. The pole of this great circle has the orientation 22°/N38° W which represents π_3 i.e. the axis of the F_3 fold in this domain. The β-diagram for this domain is more informative because it helps in determining the orientations of two regional scale limbs of the F_3 fold that forms this domain. Statistically determined structural elements from the β-diagram are as follows.

	β-diagram
Limb 1	N10° E/25° NW
Limb 2	N32° W/60° NE
S_3	N20° W/70° SW
β_3	22°/N30° W

Domain II:

This domain also depicts an open F_3 fold which lies on limbs of a tightly folded F_1/F_2 fold. Structural elements in this domain are S_0, S_1 and S_2 all of which have a general parallelism to one another. This parallelism is on account of the tightly folded F_1/F_2 folds. The domain also constitutes two limbs of F_2 folds both having almost identical orientation; both the limbs strike NE-SW and dip gently to the NW. The β-diagram for this domain gives several maxima and a single great circle with the orientation S48° W/28° N passes through them (Fig. 4.4c). This represents the average orientation of the two F_2 limbs as well as the axial plane (S_2). It is important to mention here that various maxima lying on the great circle in β-diagram either represent the various orientations of F_2 fold axes on account of rotation due to third episode of folding (F_3) or they represent the varied orientations of the F_3 axes which developed on limbs of the F_2 folds. The π-diagram for the data from this domain gives the orientation of the F_3 fold axis (π_3 = 28°/ N38° W; Fig. 4.4e).

Domain III:

Within this domain lies a macroscopic F_1 fold nose and its two limbs. The planar structural element recorded in this domain is S_0. The two macro-scale limbs of the F_1 fold have identical orientation due to the tightly folded nature of F_1. The great circle in the contoured β-diagram (Fig. 4.5c) with the orientations N97° E/20° NE

DOMAIN - I

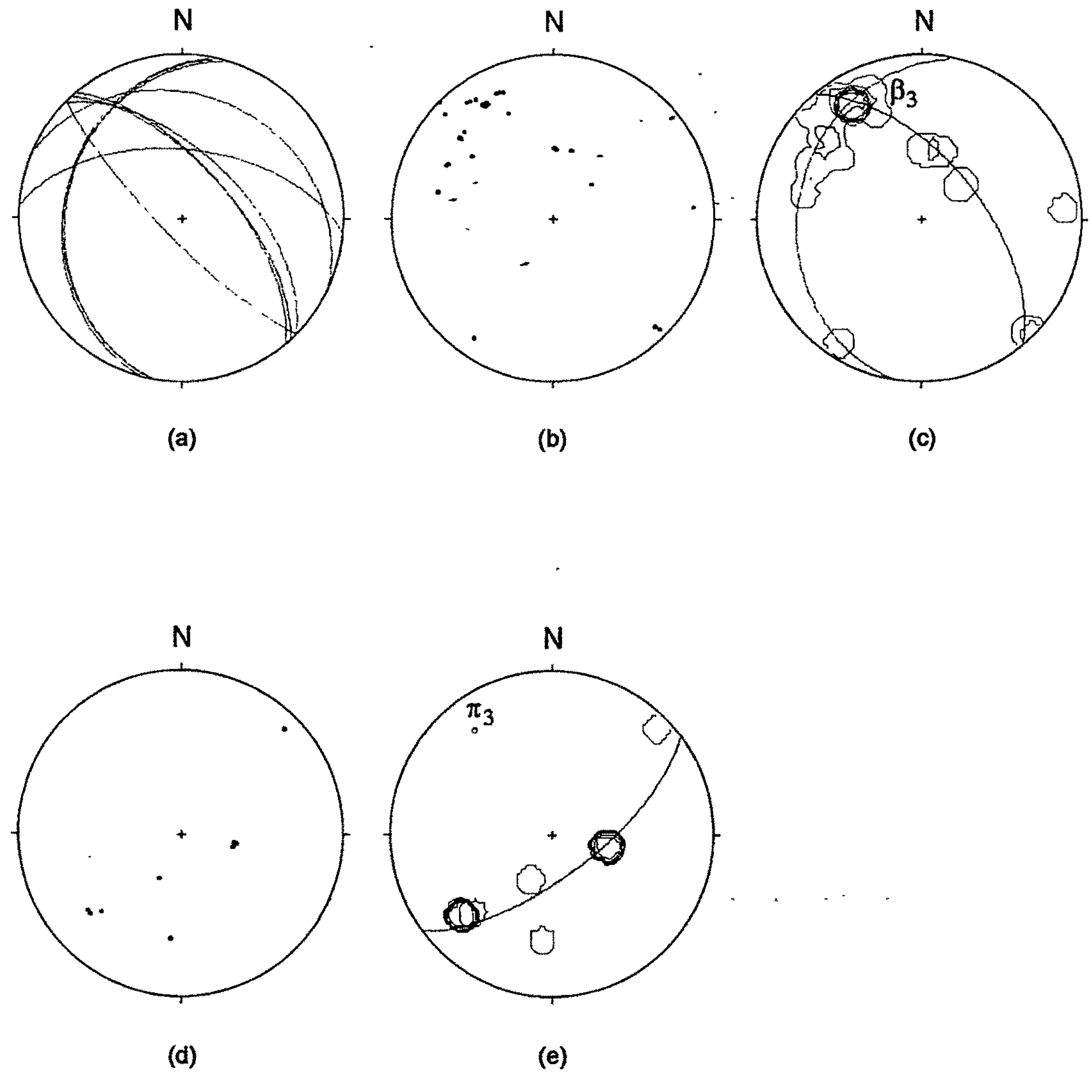

(a) Foliation surfaces as great circles (n = 9, S0, S1 and S2)
(b) β - diagram (n = 36)
(c) Contoured β – diagram; 2, 9, 16, 23, 30, 36% contours per 1% area
(d) π - diagram (n = 9, S0, S1, S2)
(e) Contoured π - diagram; 10, 15, 20, 25, 30, 35% contours per 1% area

Fig. 4.3. Structural analysis of field data from Domain I.

DOMAIN - II

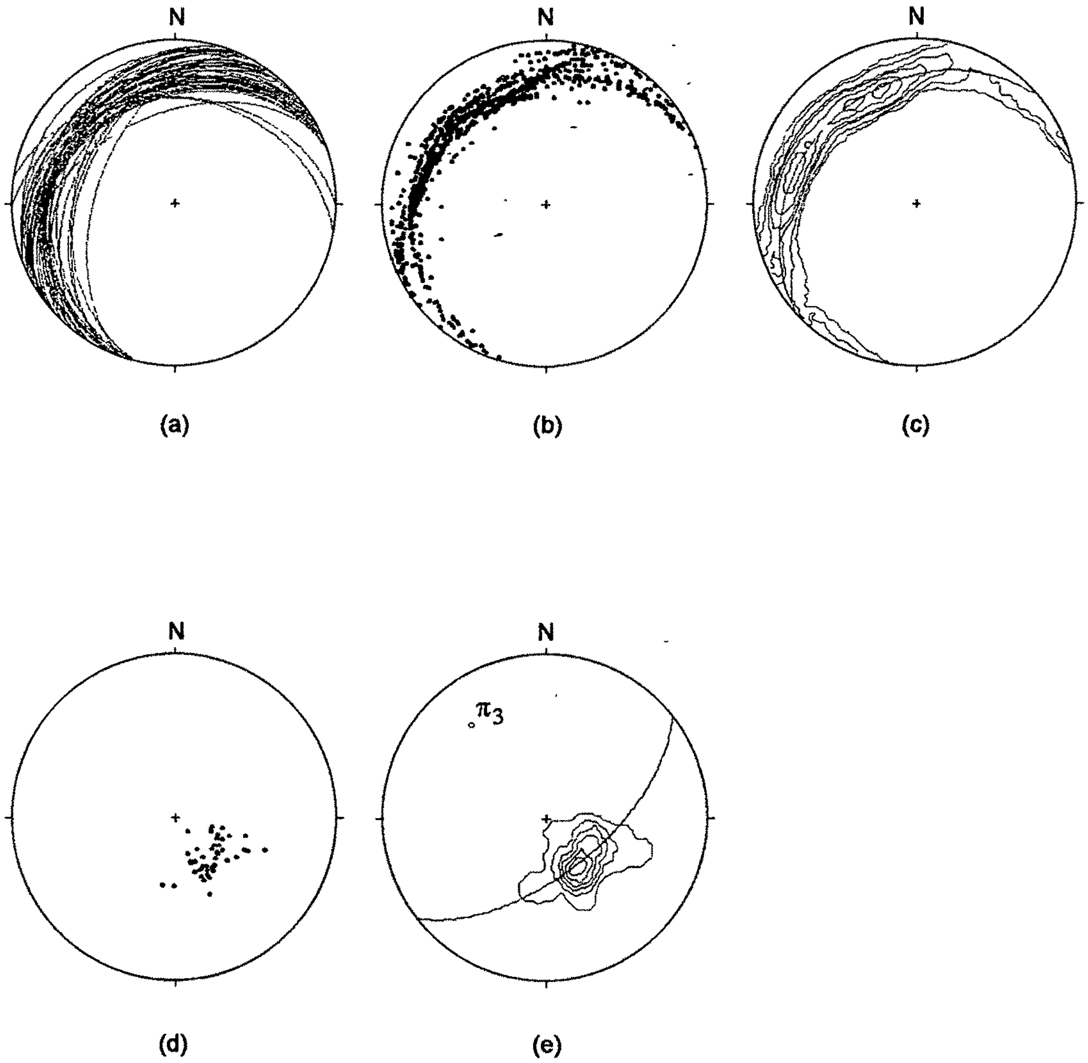

(a) Foliation surfaces as great circles (n = 46, So, S1 and S2)
(b) β - diagram (n = 1034)
(c) Contoured β – diagram; 10, 13, 17, 20, 23, 27% contours per 1% area
(d) π - diagram (n = 46, S0, S1 and S2)
(e) Contoured π - diagram; 2, 9, 13, 16, 23, 30% contours per 1% area

Fig. 4.4. Structural analysis of field data from Domain II.

DOMAIN - III

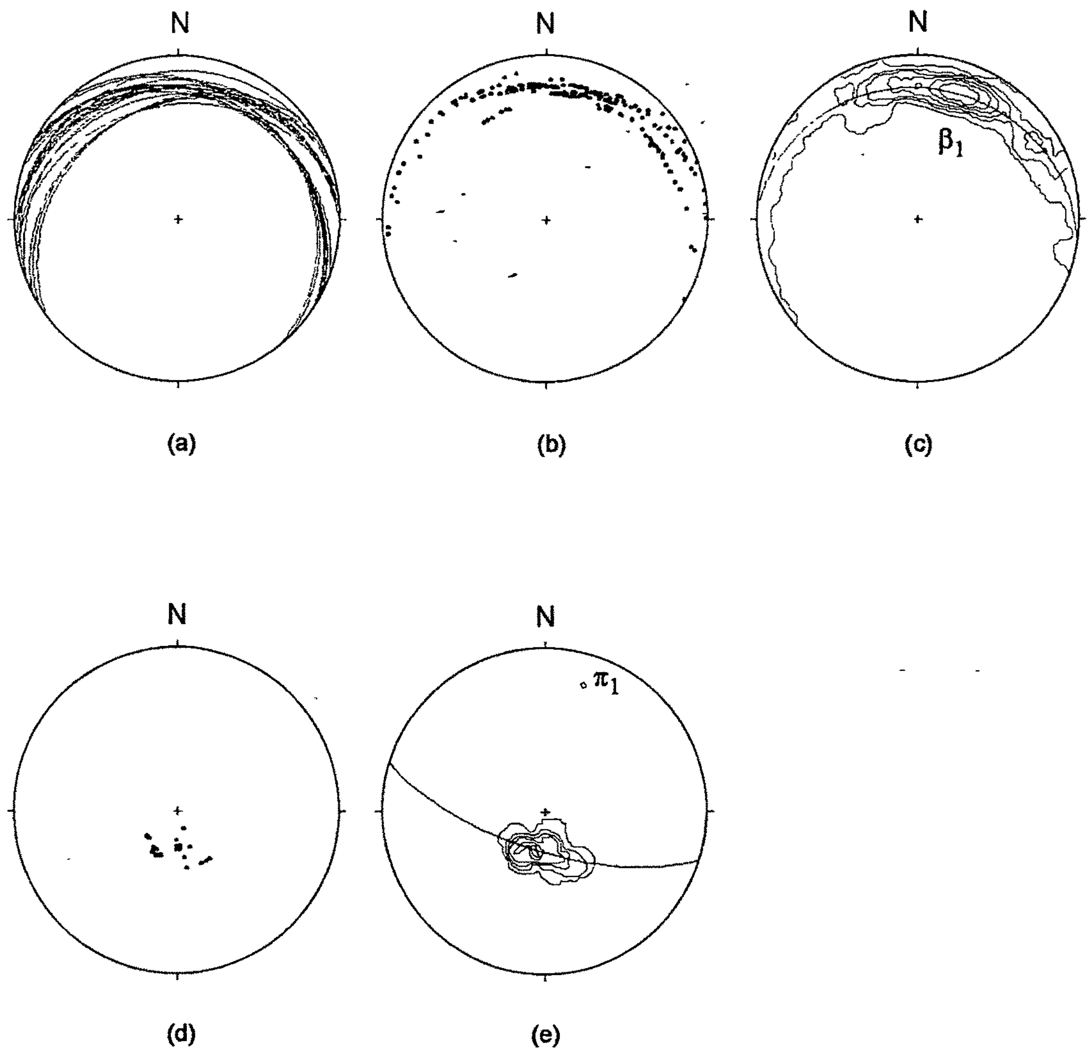

(a) Foliation surfaces as great circles (n = 20, S0)
(b) β - diagram (n = 190)
(c) Contoured β – diagram; 1, 4, 6, 9, 12, 15%contours per 1% area
(d) π - diagram (n = 20, S0)
(e) Contoured π - diagram; 5, 13, 22, 30, 38, 47% contours per 1% area

Fig. 4.5. Structural analysis of field data from Domain III.

represents the average orientation of the two F_1 limbs and the axial plane (S_1). That the fold is reclined is quite obvious from the contoured β-diagram (Fig. 4.5c) wherein the direction and amount of plunge of the F_2 fold axis (β_2 maxima in NNE direction) is identical to the direction and amount of dip of the great circle on which the β_2 maxima lies. The exact orientation of the F_1 fold axis is determined from the contoured π-diagram (Fig. 4.5e). The π_1 axis has the orientation 18°/N24° E.

It should be noted that the F_1 fold in this domain constitutes the southern limb of a large macroscopic F_2 fold, the northern limb of which falls in the domain VI to the north of the present domain. explain

Domain IV:

This domain comprises a macroscopic F_3 fold, the two limbs of which on the geological map show northeasterly and southwesterly trends respectively. The limbs show presence of bedding planes (S_0) and foliations (S_1/S_2) which have identical orientations and gentle dips. The NE-SW striking limb (i.e. southwestern limb) dips to the NW while the northeastern limb strikes NW-SE and dips to the SW. Two great circles are obtained from the β-diagram (Fig. 4.6c) which represent the statistical orientation of the limbs of the regional F3 fold. The intersection of the two great circles represents the fold axis β_3 of the F_3 fold. The axial plane (S_3) of the F_3 fold determined on the basis of the β-diagram has an orientation N108° E/80° NE. The data obtained from the structural analysis of this domain is tabulated below.

	β-diagram	π-diagram
Limb 1	N28° W/30° SW	-
Limb 2	N27° E/20° NW	-
S_3	N 72° W/80° NE	-
F_3	20°/N67° W	20°/N308° E

Domain V:

This domain consists of a open macroscopic F_3 flexure and this F_3 fold lies on the limb of a regional F_1-F_2 fold i.e. the F_3 is superimposed on limbs of the F_1-F_2 fold. Mapping has revealed that the orientations of the bedding plane and schistosity are sub-parallel. The planar structural elements on one limb are ENE-WSW to NE-SW trending with very gentle dips to the N. On the other hand, the other limb of the F_3 flexure has the planar structural elements striking NW-SE and dipping to the SW. The following are the orientations of the limbs, fold axis and axial plane from the structural analysis (Fig. 4.7).

	β-diagram	π-diagram
Limb 1	N79° E/20° NW	-
Limb 2	N36° W/40° SW	-
S_3	N56° W/79° NE	-
F_3	14° /N56° W	12° /N56° W

Domain VI:

This domain is located adjacent to domain III (i.e. N of domain III). It comprises the limb portion of a macro-scale F_2 fold (the other limb lying to the S in domain III). S_0 and S_1 are the major planar features recorded in this domain. The β-diagram (Fig. 4.8c) gives two great circles the each of which represents average orientation of S_1 over which the F_2 folds were superposed. Therefore, the

DOMAIN - IV

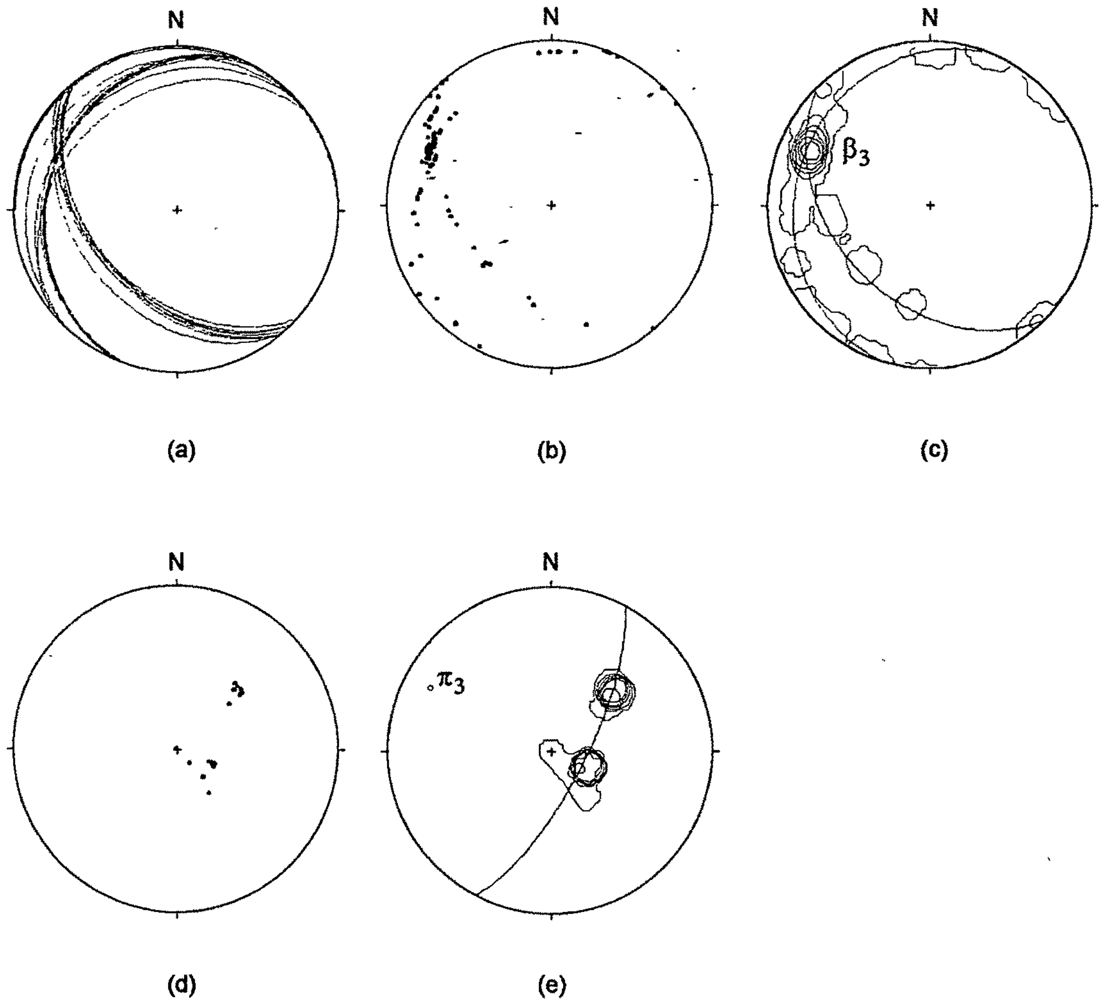

(a) Foliation surfaces as great circles (n = 16, S0 and S1)
(b) β - diagram (n = 120)
(c) Contoured β – diagram; 1, 8, 15, 22, 29, 36% contours per 1% area
(d) π - diagram (n = 16, S0 and S1)
(e) Contoured π - diagram; 6, 13, 19, 25, 31, 38% contours per 1% area

Fig. 4.6. Structural analysis of field data from Domain IV.

DOMAIN - V

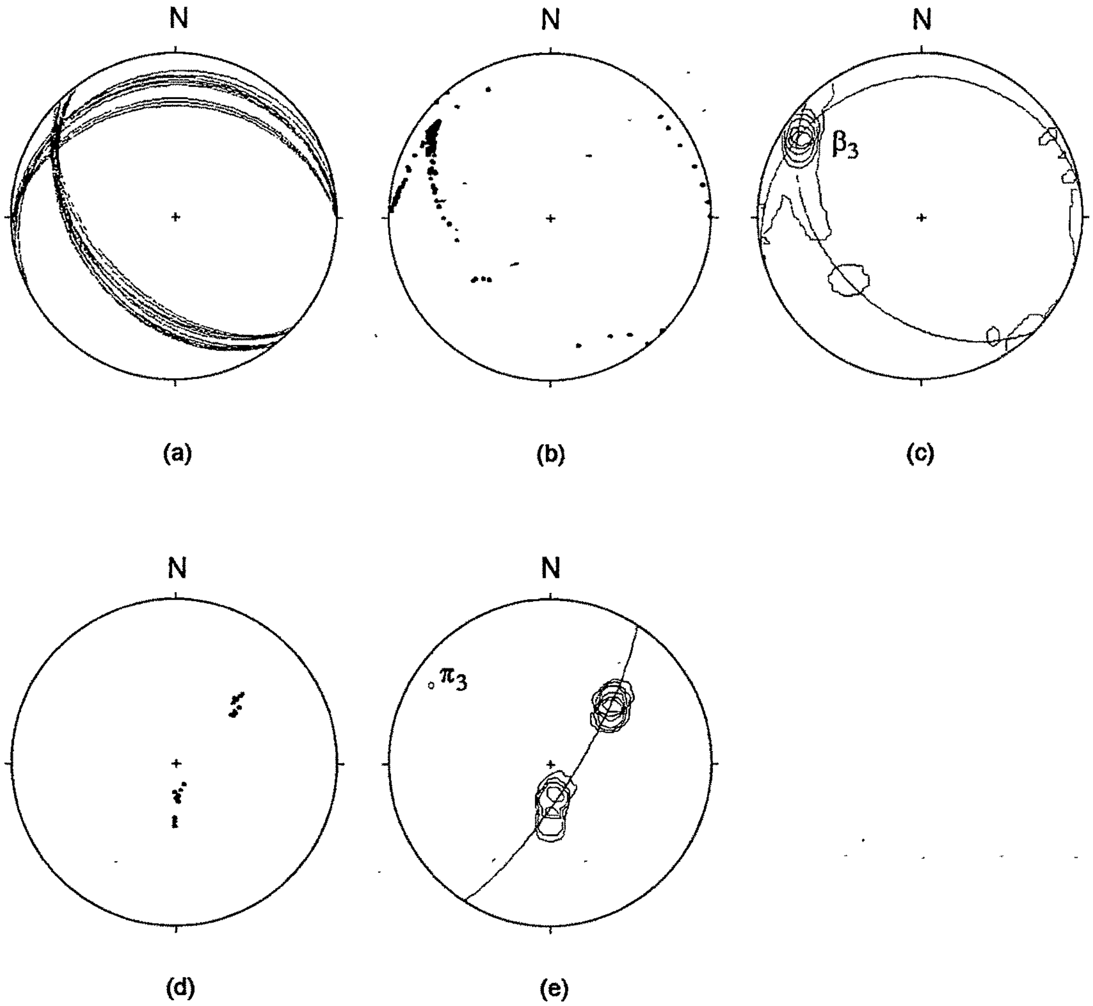

(a) Foliation surfaces as great circles (n = 19, S0, S1 and S2)
(b) β - diagram (n = 171)
(c) Contoured β – diagram; 1, 10, 20, 30, 40, 49% contours per 1% area
(d) π - diagram (n = 19 S0, S1 and S2)
(e) Contoured π - diagram; 5, 13, 21, 29, 37, 45% contours per 1% area

Fig. 4.7. Structural analysis of field data from Domain V.

DOMAIN - VI

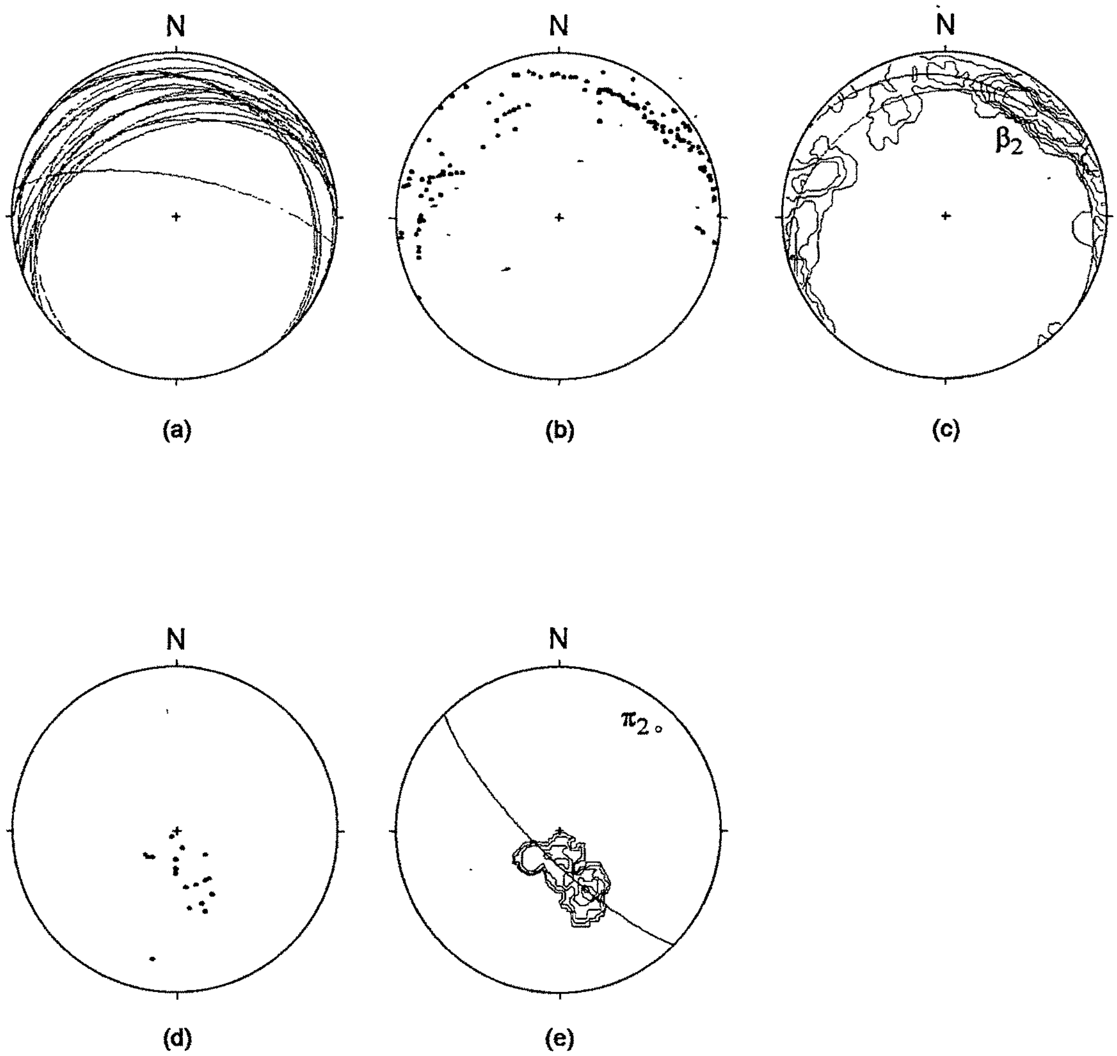

(a) Foliation surfaces as great circles (n = 18, S0 and S1)
(b) β - diagram (n = 153)
(c) Contoured β – diagram; 1, 3, 5, 7, 8, 10% contours per 1% area
(d) π - diagram (n = 18, S0 and S1)
(e) Contoured π - diagram; 6, 10, 15, 19, 24, 29% contours per 1% area

Fig. 4.8. Structural analysis of field data from Domain VI.

intersection of the two great circles gives the orientation of the F_2 fold axis (β_2). This coincides well with the F_2 (π_2-axis) determined from the contoured π-diagram (Fig. 4.8e). Moreover, the axial plane (S_2) can be determined from the β-diagram. The orientations of various structural elements determined from the structural analysis are tabulated below.

	β-diagram	π-diagram
Limb 1	N75° E/25° NW	-
Limb 2	N57° W/17° NE	-
S_2	N90° E/20° N	-
F_2	17° /N33° E	13° /N45° E

Domain VII:

This domain constitutes E-W striking S_0 and S_1 planes with moderate northerly dips. Both the above planes are sub-parallel to each other except at Anjavana where mesoscopic reclined folds are exposed. Here the schistosity (S_1) is perpendicular to S_0 (bedding plane) at the nose portions of the folds. Since most of the planar structures recorded in this domain have almost identical orientations, not much can be deciphered from the β-diagram of this domain although it clearly shows maxima in the NE quadrant (Fig. 4.9c). The π-diagram of the data-set from this domain clearly gives the exact orientation of the F_2 fold axis (π_2 = 28°/N57° E; Fig. 4.9e).

The author has separated the readings of the S_0 planes of the mesoscopic F_1 reclined folds occurring at Anjavana from the data-set of the entire domain VII and plotted them separately in Fig. 4.10. The reclined nature of these folds is well revealed from the contoured β-diagram (Fig. 4.10c). The pole to the best fit great circle in Fig. 4.10e (π-diagram) represents the F_1 fold axis of the reclined fold. This axis (π_1) coincides well with the orientation of F_2 axis (π_2) for the entire domain VII (Fig. 4.9e). This indicates that the F_1 and F_2 folds were coaxial.

Domain VIII :

Structural data recorded from this domain is rather inadequate for making conclusive interpretations. The β and π-diagrams for the planar structural elements of this domain give several maxima which might represent different orientations of F_1, F_2 and F_3 axes. Due to inadequate data from this domain, it has not been possible to separate the maxima related to axes belonging to the different fold events. However, it is worth mentioning here that the π-girdle in Fig. 4.11e (π-diagram) gives a pole (representing the -axis) plunging due NNE. This probably represents F_1-F_2 fold axis. On the other hand, there is a spread in maxima in NNE-SSW direction (Fig. 4.11e) which could be on account of F_3 folding.

Domain IX :

This domain constitutes the easternmost extremity of the study area. Two limbs of a macroscopic F_3 fold comprise this area. On the basis of mapping of structural elements, it is found that the bedding planes on one limb strike N-S and dip steeply to the W. Bedding planes on the other limb strike almost E-W and dip gently to the N. Intersection of the two limbs gives the orientation of F_3 axis (β_3) (Fig. 4.12c). The structural data determined from analysis are as follows.

	β-diagram	π-diagram
Limb 1	N15° W/63° WSW	-
Limb 2	N76° E/30° NNW	-
S_3	N43° W/68° NE	-
F_3	28° /N30° W	33° /N25° W

It is to be noted that several minor maxima lie on each limb of F_3 fold in β-diagram (Fig. 4.12c) which probably represent the varying orientations of F_1/F_2 axis lying on the F_3 limbs.

Domain X :

This domain on the map shows a F_2 fold comprising its two limbs and the core. The northern limb strikes in NE-SW direction while the southern limb strikes almost due E-W direction. The β-diagram (Fig. 4.13c) shows a maxima (F_2 axis) in the NE quadrant. The exact orientation of the F_2 axis is obtained from the π-diagram wherein π_2 = 20° /N25° E. It is important to mention here that this domain forms the western portion of an F_3 closure such that an overall shallow basinal depression is formed in the region to the N of Lunavada-Santrampur tract. This fact is better understood when the data from domain XI lying to the east of this domain are taken into account.

Domain XI :

The region lying to the N of river Mahi which comprises the sub-region I described in Chapters 3 and 4 has been considered as domain XI. It constitutes folded quartzite ridges clearly showing presence of F_2 folds on a regional scale. This domain is further sub-divided from N to S into three sub-domains.

Sub-domain XIa : Area around Ditwas

Sub-domain XIb : Area around Godhar

Sub-domain XIc : Area around Ghasvada

The data of planar structures (S_0 and S_1) recorded in the field were analysed separately for each sub-domain to obtain positions of the F_2 fold axis (β_2) and F_2 axial plane (S_2) for each sub-domain.

Sub-domain XIa: The structural analysis for this sub-domain which comprises a macroscopic F_2 fold reveals that the axial plane (S_2) strikes almost N-S with a gentle dip towards the W and the fold axis plunges gently to the SW (Fig. 4.14). The results of β- and π-diagrams are as follows.

	β-diagram	**π-diagram**
Limb 1	N45° E/38° NW	-
Limb 2	N60° W/25° SW	-
S_2	N72° E/82° SE	-
F_2	19° /S73° W	23° /S75° W

The maxima in the NW quadrant of the β-diagram might be representing F_1 or F_3 axis on the limb of F_2. Moreover, it is worth mentioning that the author came across a few well sections around Ditwas in the field which show presence of vertical axial plane fractures (S_2). These have been plotted on the structural map of the study area (Fig. 4.1).

Sub-domain XIb: This sub-domain also consists of an F_2 fold with the fold axis plunging gently to the SW and the axial plane striking NE-SW with steep dip (sub-vertical). Orientations of two limbs of the macro-scale folds and the fold axis (β_2) can be obtained from the β-diagram (Fig. 4.15c). Moreover, the π-diagram (Fig. 4.15e) also gives the orientation of the fold axis (π_2 = 35° / N210° SSW) which coincides well with the β_2-axis. The π-diagram for this sub-domain however is not very informative and shows several separated maxima.

	β-diagram	**π-diagram**
Limb 1	N5° E/55° WNW	-
Limb 2	N45° W/35° SW	-
S_2	N43° W/67° SE	-
F_2	36° / S35° W	35° / S30° W

Sub-domain XIc: The structural information derived from the β- and π-diagrams (Fig. 4.16) of this sub-domain is as follows.

	β-diagram	π-diagram
Limb 1	N6° E/52° WNW	-
Limb 2	N35° W/52° SW	-
S_2	N75° E/90	-
F_2	44° /S54° W	45° /S65° W

As is seen from the above three sub-domains, the fold axis of the F_2 folds plunges gently to the SW with only minor variations in different sub-domains, the variations are attributed to be an effect of F_3 folding. The synoptic β- and π-diagrams of the entire domain XI (Fig. 4.17) also gives a F_2 axis plunging in the SW direction. Nose of a mesoscopic F_2 fold with the axis plunging gently due SW is exposed on a road cutting near Munpur (Fig. 3.5) and this fits very well with the orientation of the fold axis determined from the analysis of structural data.

DOMAIN - VII

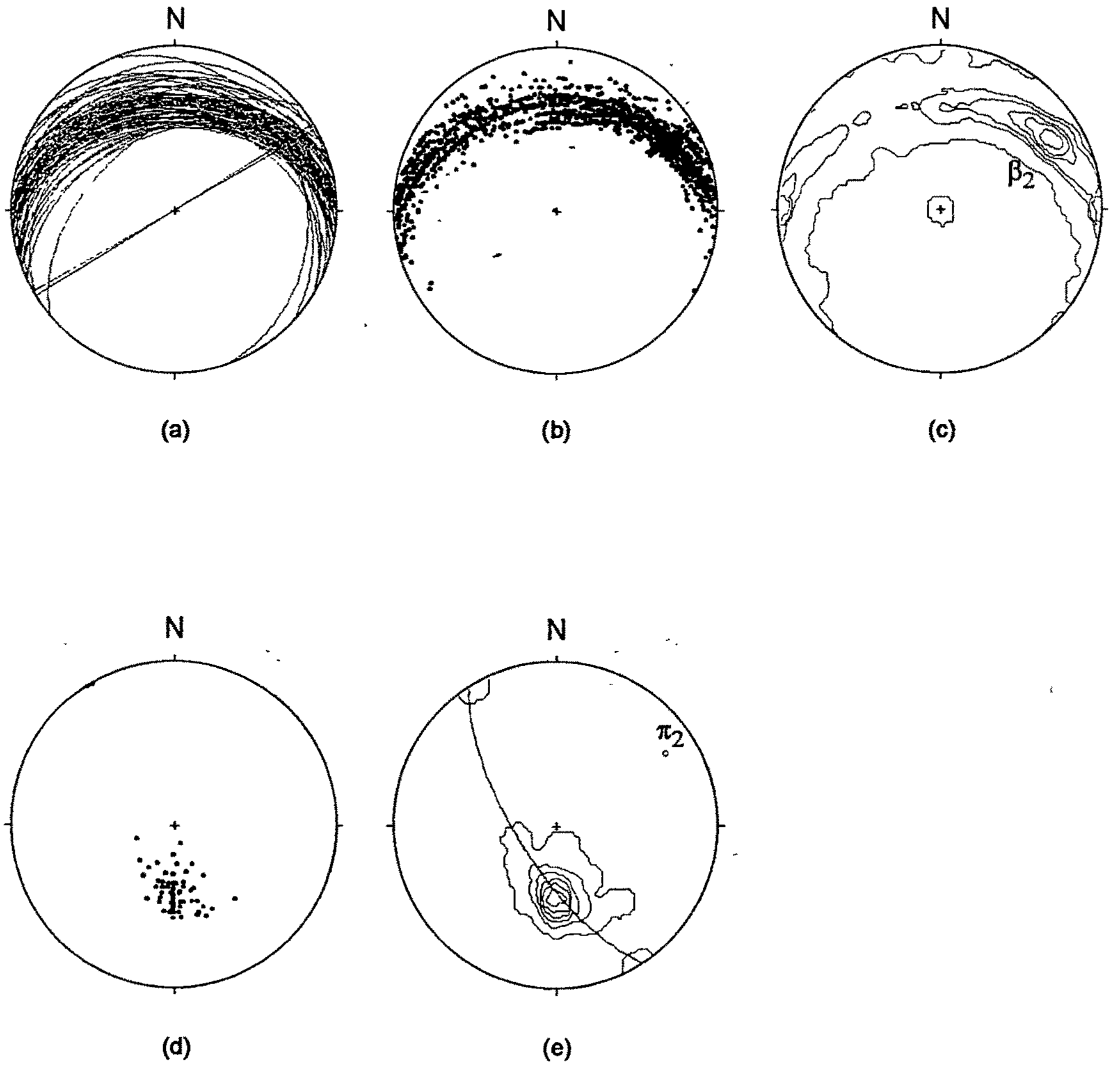

(a) Foliation surfaces as great circles (n = 67, S0 and S1)
(b) β - diagram (n = 2204)
(c) Contoured β – diagram; 1, 3, 5, 8, 10 and 13% contours per 1% area
(d) π - diagram (n = 67, S0 and S1)
(e) Contoured π - diagram; 1, 9, 16, 23, 30 and 38% contours per 1% area

Fig. 4.9. Structural analysis of field data from Domain VII.

F1 RECLINED FOLD (ANJAVANA)

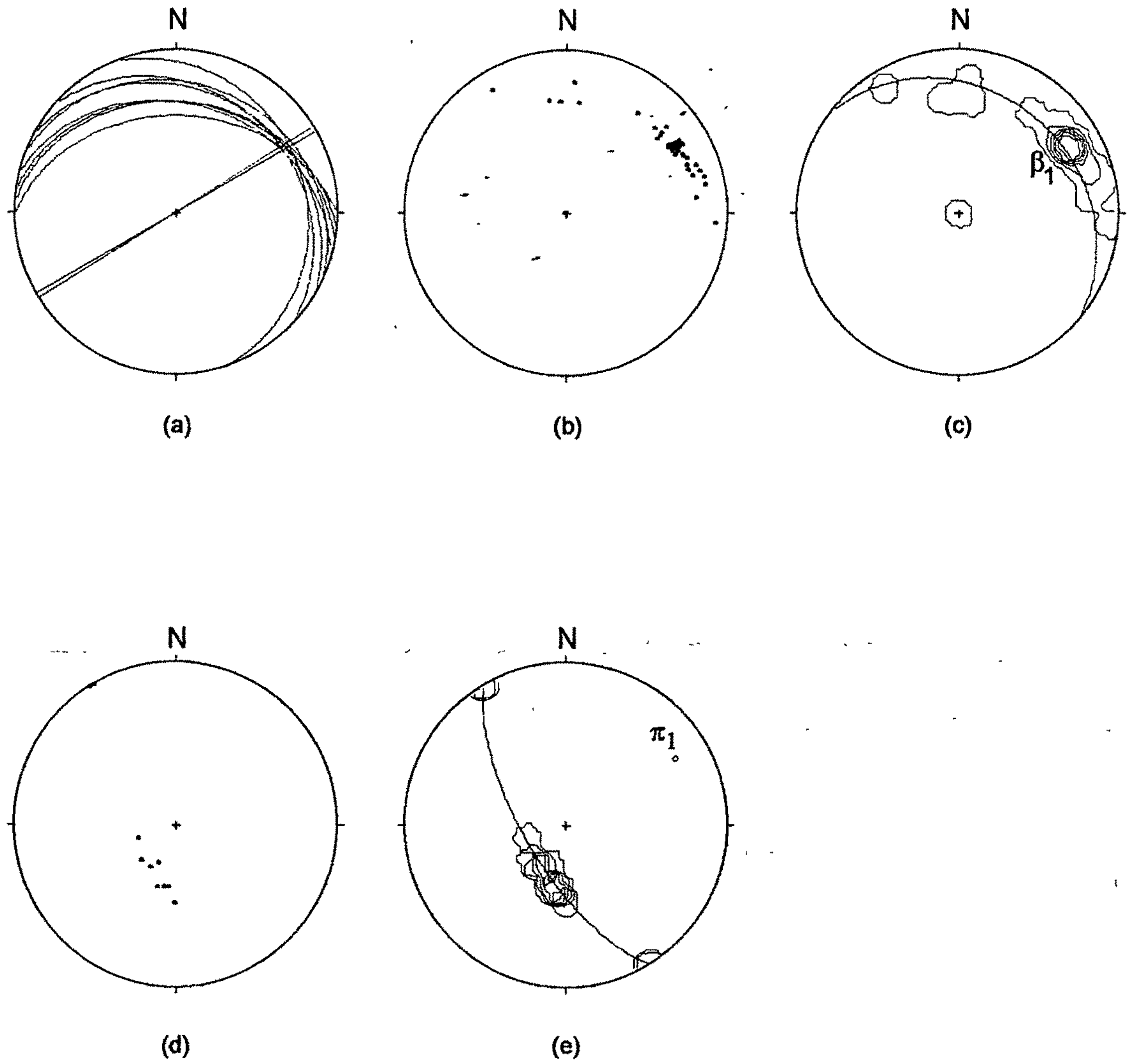

(a) Foliation surfaces as great circles (n = 10, S0)
(b) β - diagram (n = 45)
(c) Contoured β – diagram; 10, 17, 23, 30, 37, 43% contours per 1% area
(d) π - diagram (n = 10, S0)
(e) Contoured π - diagram; 2, 11, 21, 30, 39, 49% contours per 1% area

Fig. 4.10. Structural analysis of field data of reclined fold located at Anjavana in Domain VII.

DOMAIN - VIII

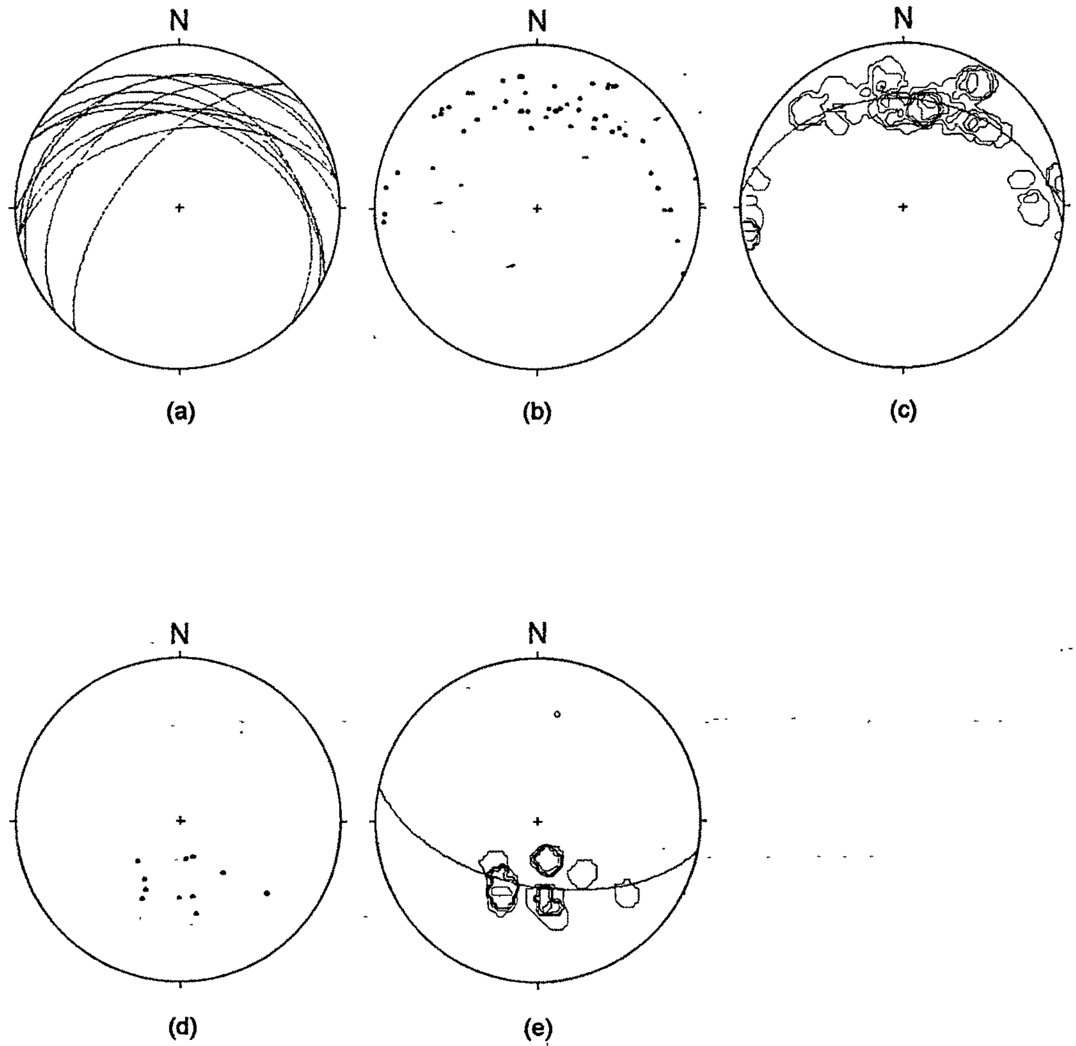

(a) Foliation surfaces as great circles (n = 11, S1 and S2)
(b) β - diagram (n = 55)
(c) Contoured β – diagram; 2, 4, 6, 8, 10, 12% contours per 1% area
(d) π - diagram (n = 11, S1 and S2)
(e) Contoured π - diagram; 9, 12, 15, 18, 21, 24% contours per 1% area

Fig. 4.11. Structural analysis of field data from Domain VIII.

DOMAIN - IX

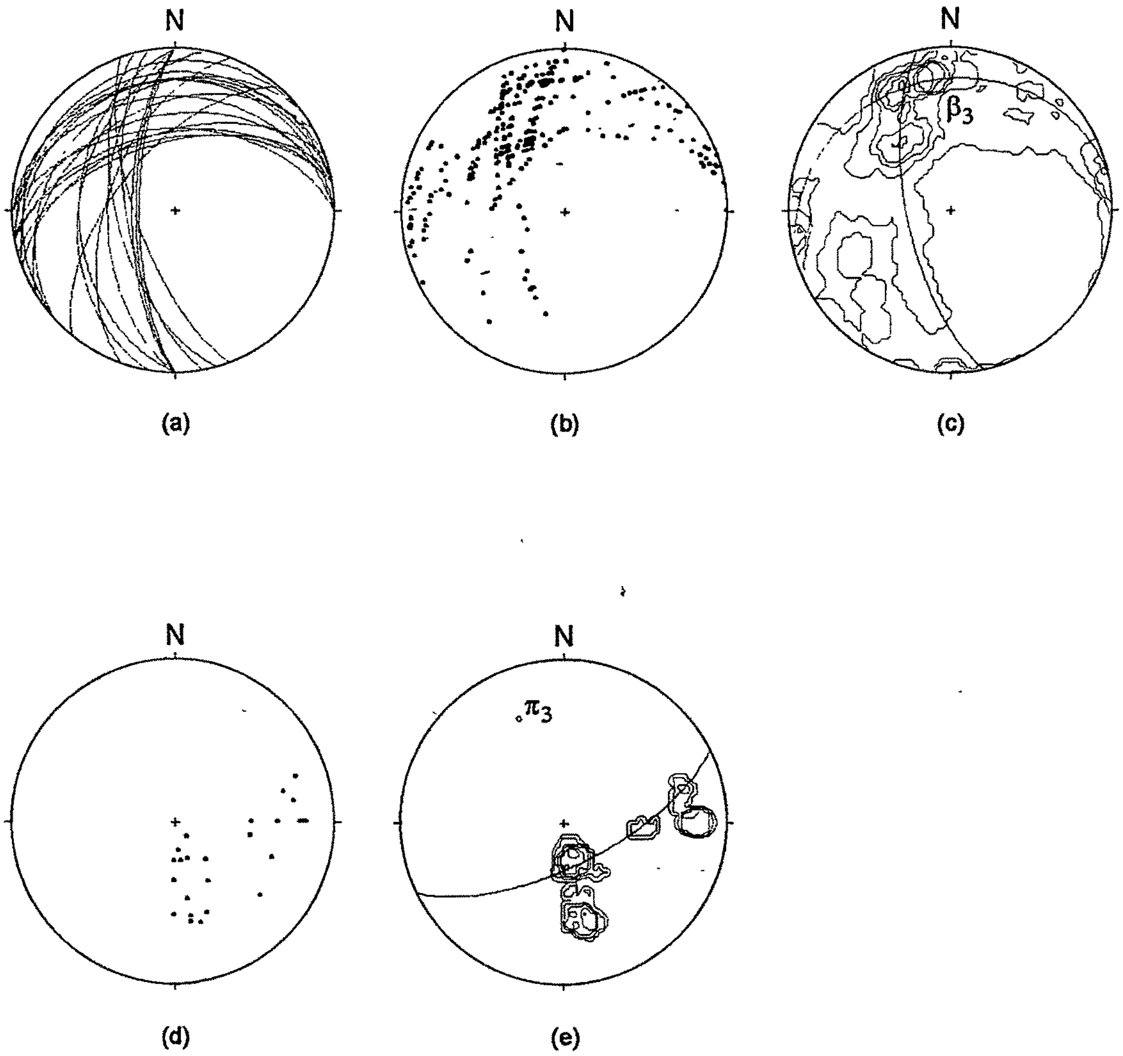

(a) Foliation surfaces as great circles (n = 26, S0 and S1)
(b) β - diagram (n = 324)
(c) Contoured β – diagram; 1, 2, 4, 6, 8, 10% contours per 1% area
(d) π - diagram (n = 26, S0 and S1)
(e) Contoured π - diagram; 4, 7, 10, 13, 17, 20% contours per 1% area

Fig. 4.12. Structural analysis of field data from Domain IX.

DOMAIN - X

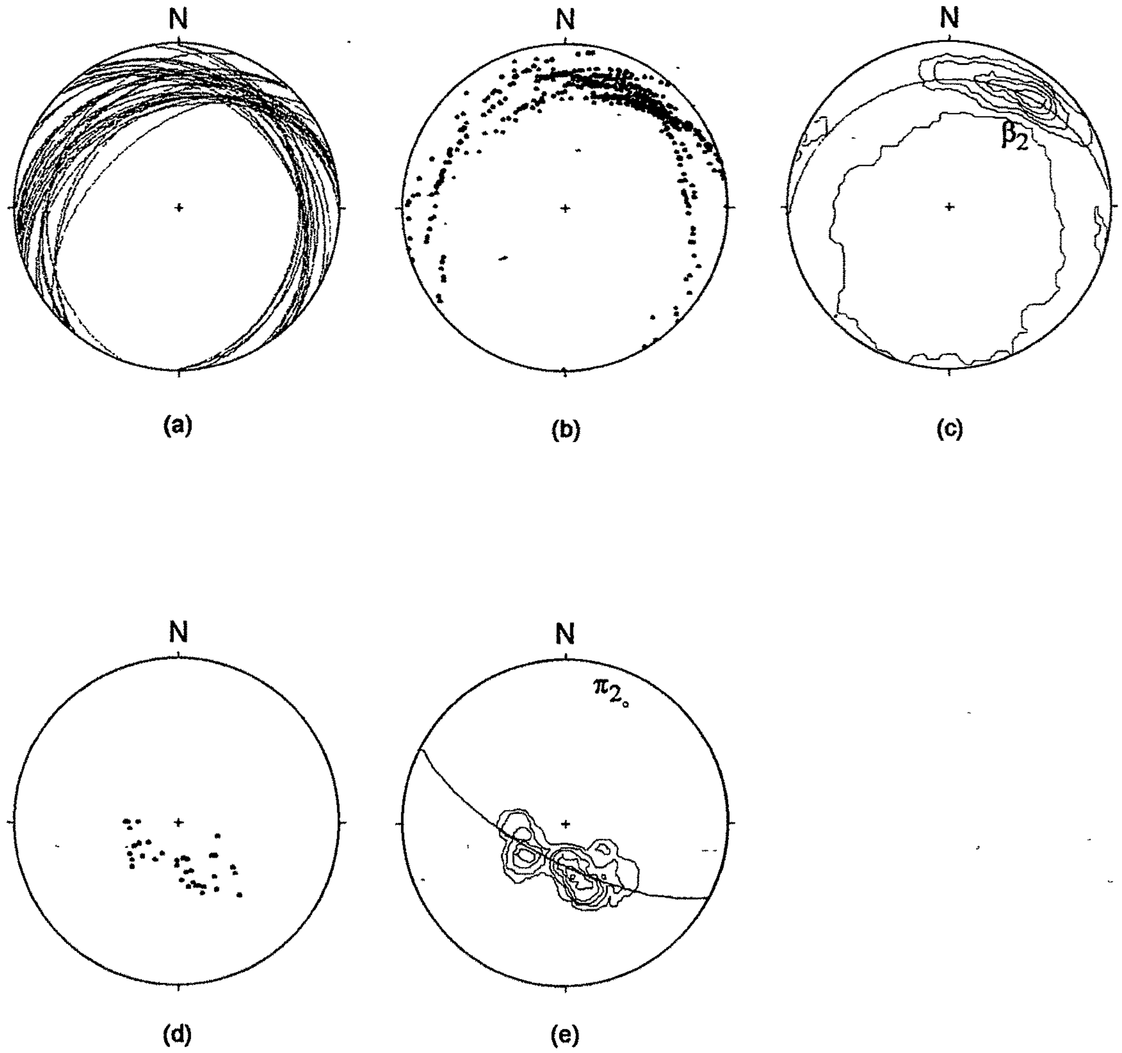

(a) Foliation surfaces as great circles (n = 36, S0 and S1)
(b) β - diagram (n = 630)
(c) Contoured β – diagram; 1, 3, 6, 9, 12, 15% contours per 1% area
(d) π - diagram (n = 36, S0 and S1)
(e) Contoured π - diagram; 3, 7, 12, 17, 21, 26% contours per 1% area

Fig. 4.13. Structural analysis of field data from Domain X.

DOMAIN - XIa (DITWAS)

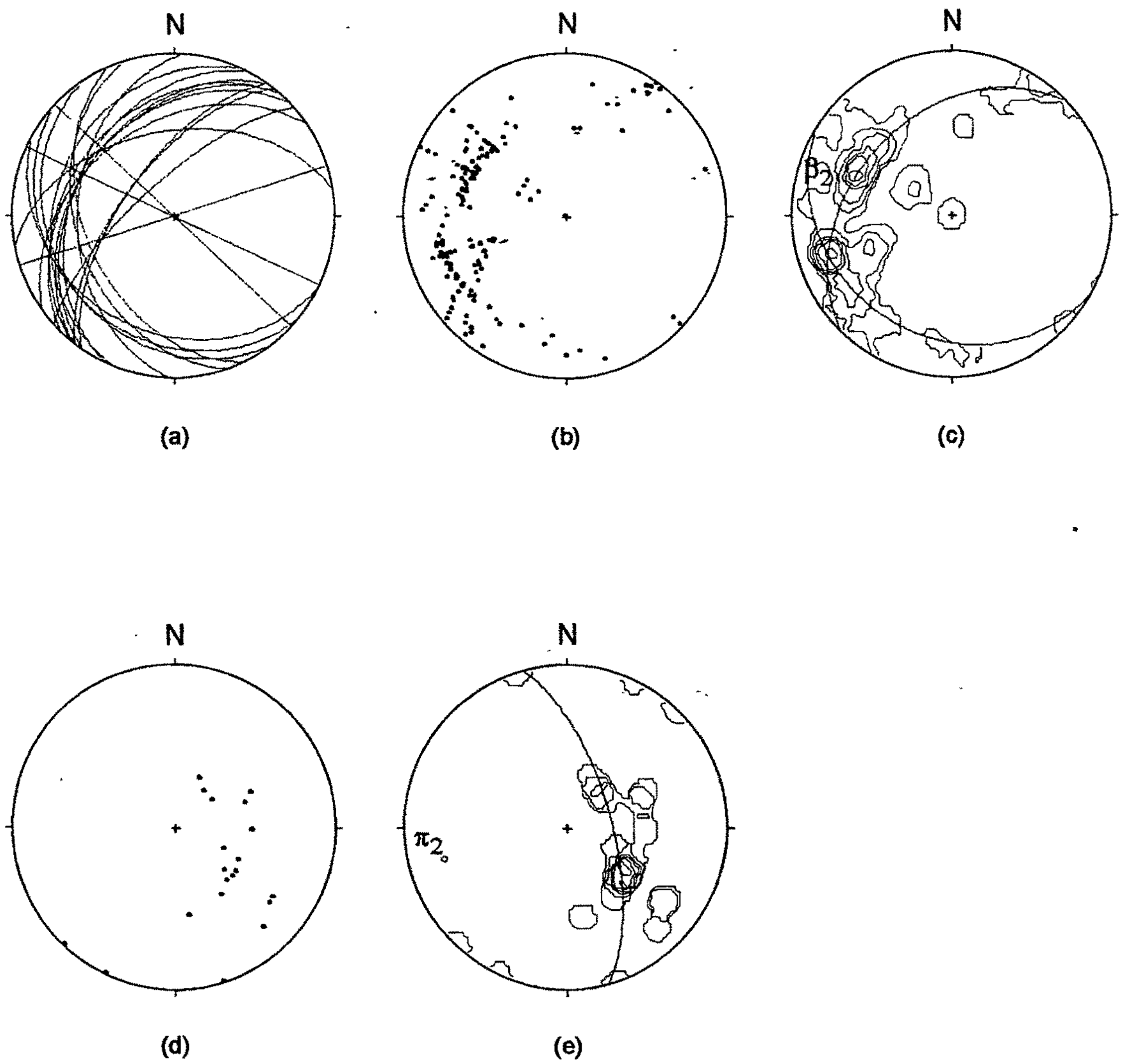

(a) Foliation surfaces as great circles (n = 20, S0 and S1)
(b) β - diagram (n = 190)
(c) Contoured β – diagram; 1, 3, 6, 9, 12, 15% contours per 1% area
(d) π - diagram (n = 20, S0 and S1)
(e) Contoured π - diagram; 5, 8, 12, 15, 18, 22% contours per 1% area

Fig. 4.14. Structural analysis of field data from Domain XIa.

DOMAIN XI b (GODHAR)

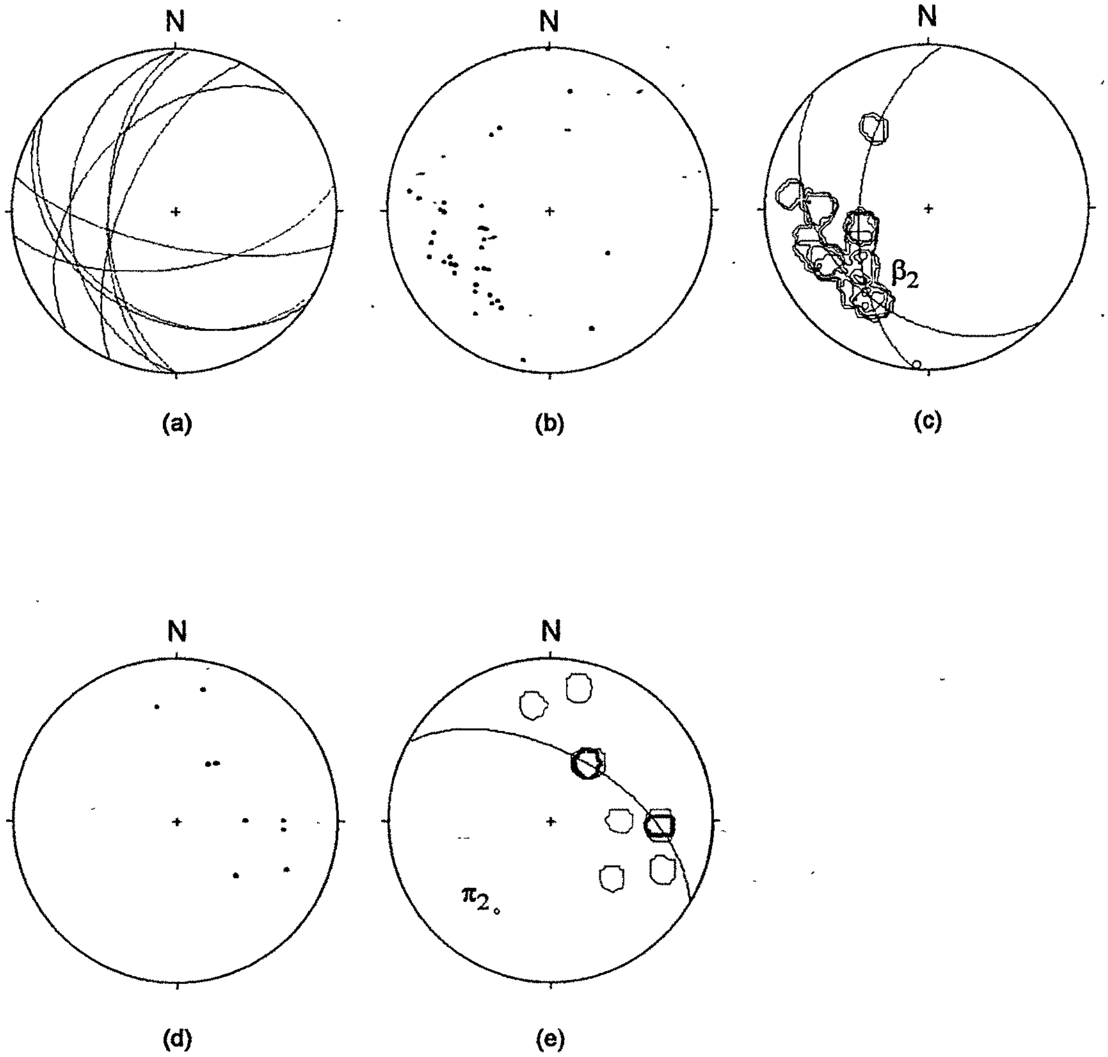

(a) Foliations as great circles (n = 9, S0 and S1)
(b) β - diagram (n = 36)
(c) Contoured β – diagram; 3, 4, 7, 10, 12, 14% contours per 1% area
(d) π - diagram (n = 9, S0 and S1)
(e) Contoured π - diagram; 11, 13, 15, 17, 19, 20% contours per 1% area

Fig. 4.15. Structural analysis of field data from Domain XIb.

DOMAIN XIc (GHASVADA)

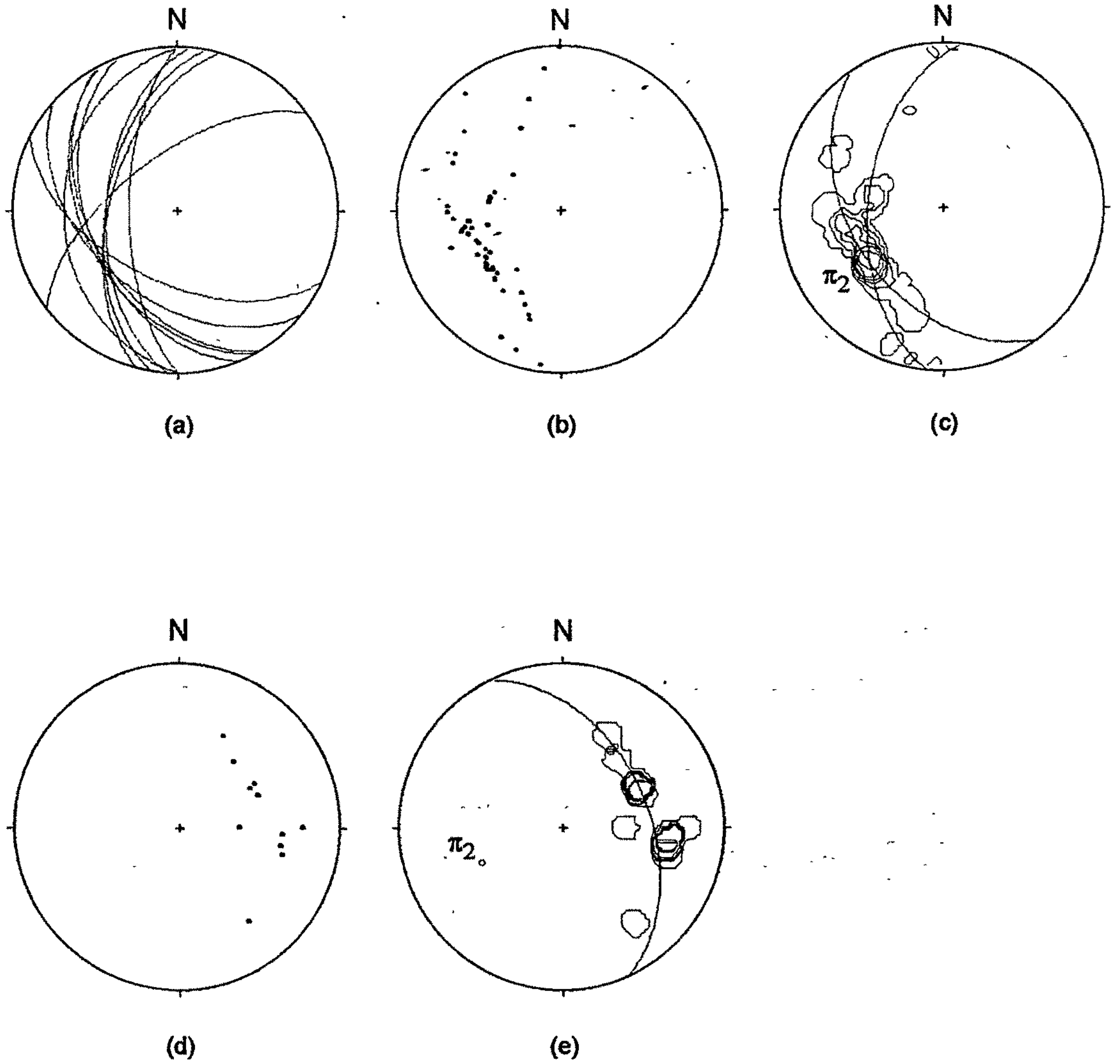

(a) Foliation surfaces as great circles (n = 11, S0 and S1)
(b) β - diagram (n = 55)
(c) Contoured β – diagram; 9, 12, 15, 18, 21, 24% contours per 1% area
(d) π - diagram (n = 11, S0 and S1)
(e) Contoured π - diagram; 2, 7, 12, 16, 21, 26% contours per 1% area

Fig. 4.16. Structural analysis of field data from Domain XIc.

DOMAIN - XI

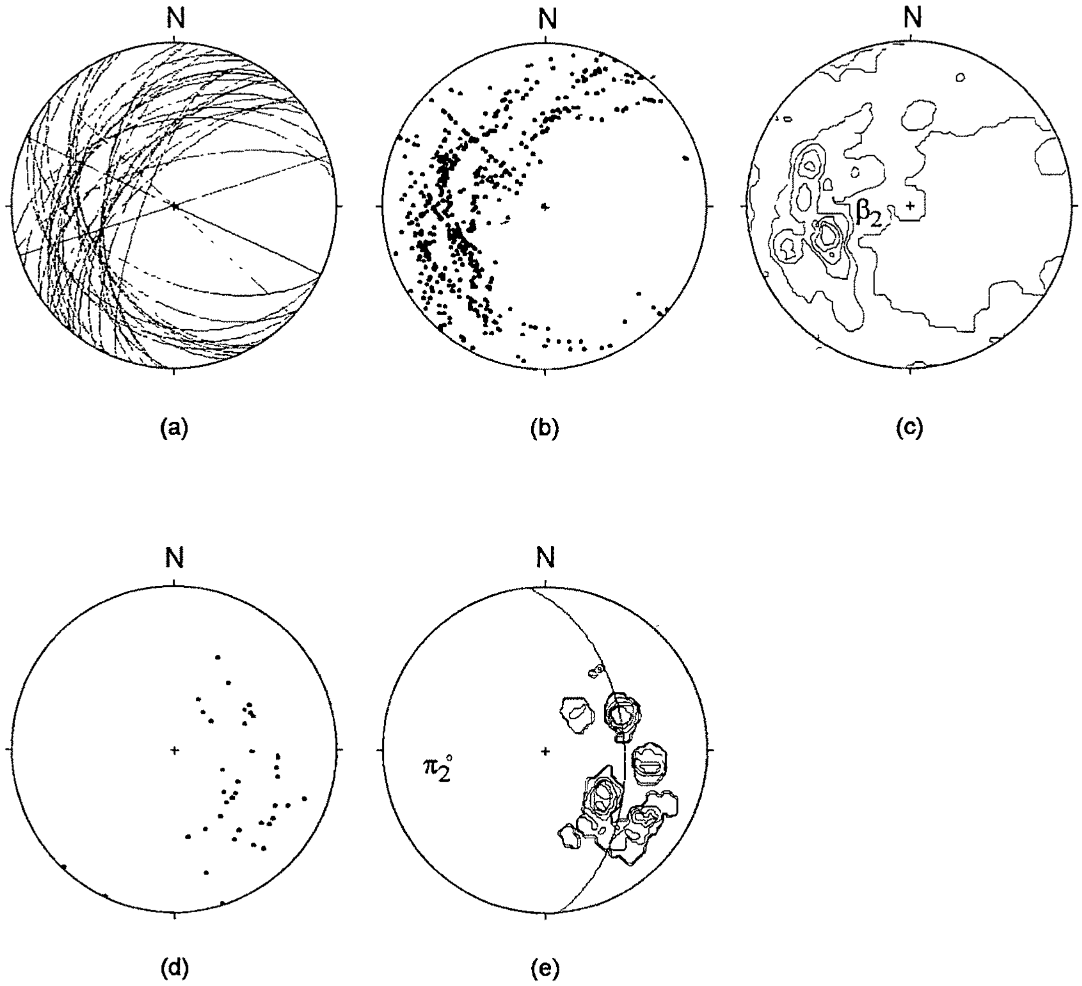

(a) Foliation surfaces as great circles (n = 38, S0 and S1)
(b) β - diagram (n = 703)
(c) Contoured β – diagram; 1, 2, 4, 6, 8, and 10 % contours per 1% area
(d) π - diagram (n = 38, S0 and S1)
(e) Contoured π - diagram; 3, 4, 6, 8, 10, and 11% contours per 1% area

Fig. 4.17. Structural analysis of field data from the entire Domain XI.

Domain XII :

Field exposures are inadequate field exposures in this domain as a result of which the data recorded in the field was insufficient to carry out stereographic analysis. However, the data collected from a few exposed areas suggests that the rocks here have horizontal bedding planes. Also at Dolatpura on the banks of river Mahi, NE-SW trending recumbent F_2 folds (Fig. 3.7) were observed.

4.4. STRUCTURAL SYNTHESIS

The β- and π-diagrams for the 12 domains have enabled the author to appropriately classify and categorize macroscopic and mesoscopic folds belonging to successive events. Of course, on account of paucity of adequate small folds related to the three deformations and also due to scarcity of preserved beddings and axial plane cleavages, the stereograms had to be interpreted keeping in mind the overall outcrop pattern of the quartzite ridges. Figs. 4.18 and 4.19 show the orientations of the different fold axes in the study area established on the basis of structural analysis. The structural picture that has emerged from the analysis of data is marked by the following characteristics.

1. The Pre-Cambrian rocks around Lunavada and Santrampur have undergone three episodes of deformation D_1, D_2 and D_3 which resulted in the development of F_1, F_2 and F_3 folds. The F_1 and F_2 folds have NE-SW trend and are coaxial while the F_3 folds have a NW-SE to WNW-ESE trend.

Why not both have same.

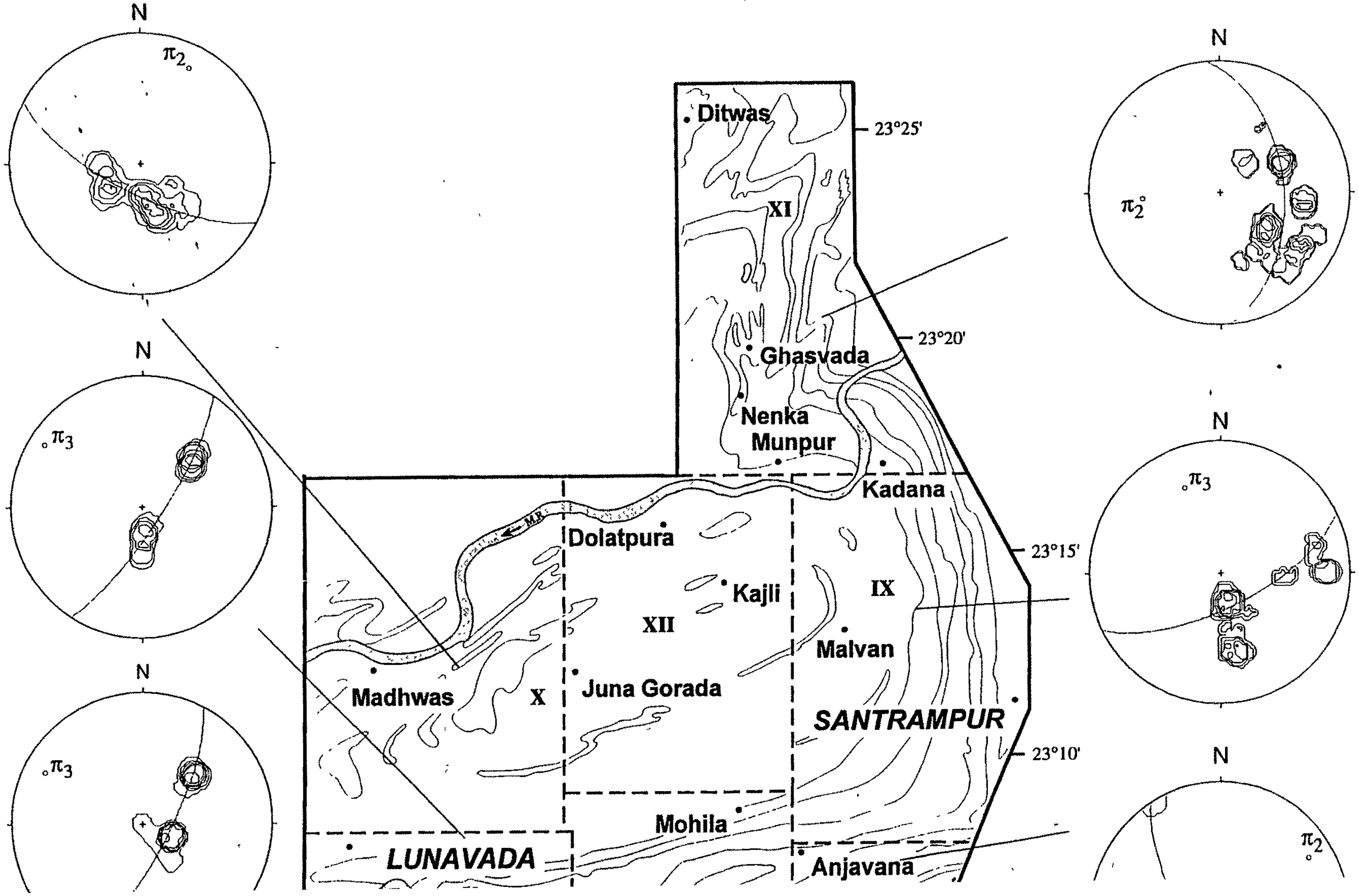
N
π2
π3
Ditwas
XI
23°25'
23°20'
Ghasvada
Nenka
Munpur
Kadana
23°15'
Dolatpura
Kajli
XII
IX
Malvan
Madhwas
X
Juna Gorada
SANTRAMPUR
23°10'
Mohila
LUNAVADA
Anjavana
MR

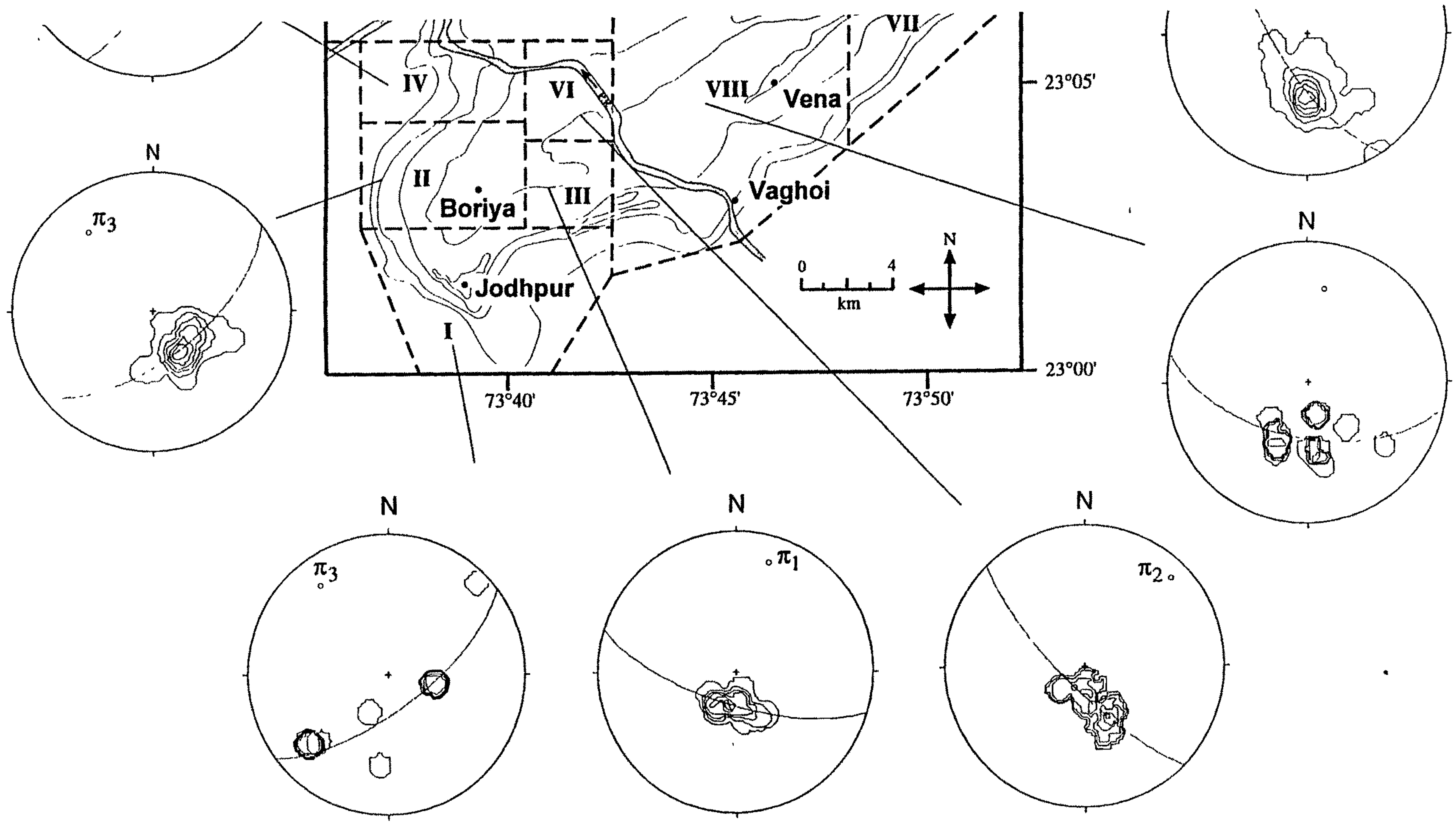

Fig. 4.18. Map showing π-diagrams for the various structural domains of the study area.

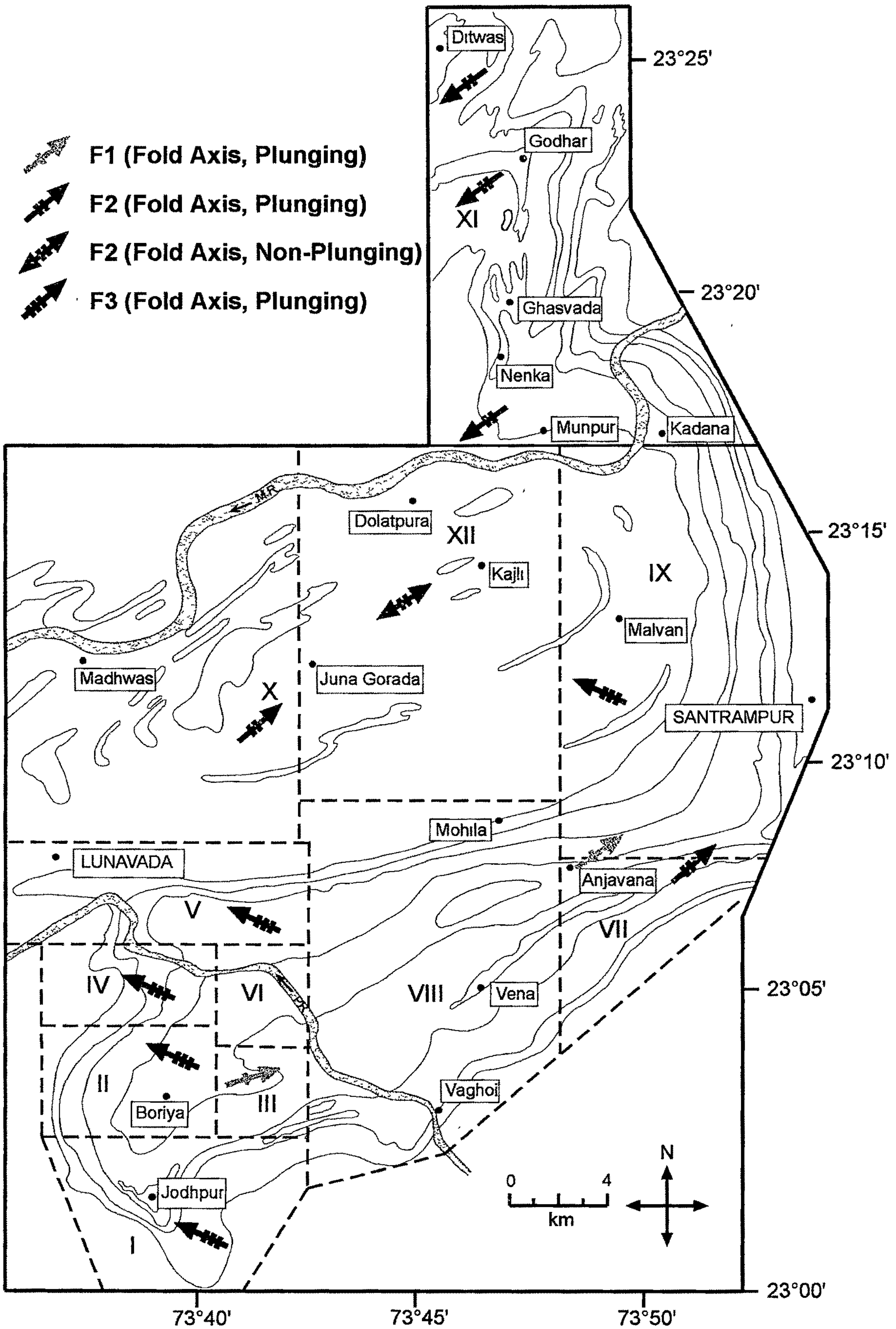

Fig.4.19. Map showing the orientations of statistically determined fold axes in the various structural domains of the study area

2. The interference of the three fold events has given rise to unique regional outcrop pattern pointing to superposition of various fold events in different combinations. The geological and structural map of the area and also the trends of ridges on the satellite imagery ideally reveal this interference phenomenon. The central part of the area shows a regional scale Type-III interference pattern due to superposition of NW-SE trending open F_3 fold over NE-SW trending F_1/F_2 isoclinal folds. The region to the S of Lunavada-Santrampur tract shows a megascopic Type-I interference pattern due to superposition of F_1 and F_2 folds, the two fold events being coaxial with NE-SW trend.

3. The rocks in the northern part (i.e. sub-region I in Chapters 3 and 4) show effects of F_2 folding on F_1. This fact is ideally seen in the geomorphic and geological map. In this context it is relevant to make a few generalizations in respect of the area to the W where very conspicuous ENE-WSW trending quartzite ridges (satellite image, Fig. 3.1) are encountered. Though this portion lies outside the study area, it can be undoubtedly stated that here the rocks show a good example of coaxial isoclinal F_1-F_2 folding. The effect of F_3 in the northern part is not so conspicuous as compared to that in the areas to the S of the Mahi river; however, the minor variations in the orientations of F_2 axis, as seen in the various sub-domains of domain XI are attributed to F_3 folding.

4. The rocks in the central part of the study area including domains IX, X and XII show very ideally the interference of F_1 and F_2 and F_1-F_2 with F_3. The outcrop pattern and the satellite imagery data exhibit macroscopic F_2 fold in the western part of domain X The eastern part falling within domain IX however, shows

effects of F_3 folding; though earlier folds are present, they are not easily identifiable. Generally speaking the westernmost part comprises nose of a F_2 fold, the dips of both the limbs of which are in northerly direction. The F_2 fold axis plunges due NE. The median portion of this area constituting domain XII which has scarce exposures, is however found to contain F_2 recumbent folds with NE-SW trend. The eastern portion illustrates a very distinct open F_3 fold whose two limbs are respectively trend ENE-WSW and N-S, with dips to the N and W respectively. The F_3 axis plunges gently to the NW. The F_2 folds do not come out well on any of the stereograms but the repetitive outcrop pattern of quartzite ridges and some very tight closures are evidences of F_1 and F_2 folds. Some of the maxima seen on the contoured β-diagrams (domain IX; Fig. 4.12) indicate different positions of F_1-F_2 axis. On integrating the structural data from the different parts of the region to the S and N of the Mahi, it is found that from W towards ENE i.e. from domain X to XII to XI, the direction of plunge of the F_2 axis changes from NE through horizontal to SW respectively (Fig. 4.18 and 4.19). This variation in the attitude of the F_2 axis is an effect of the F_3 folding, resulting into a regional synformal/ basinal structure in the area comprising sub-region II (S of Mahi). Domains XI and X represent the northeastern and western limbs of a large scale open F_3 fold and the nose portion of the fold is represented by domain XII.

5. Southernmost part of the study area is structurally the most complex. The regional outcrop pattern itself reveals the imprints of three fold events, F_1, F_2 and F_3. The outcrop configuration in the western half of this part of the study area comprising seven domains (domain I to VII) illustrates more or less coaxial and

coplanar F_1 and F_2 interference. The F_3 fold here is a antiform, to the east of which are located smaller F_3 synforms and antiforms. Easternmost part consisting of domain VII and part of domain IX to its north show a outcrop pattern wherein two limbs of a major F_2 fold are seen to have been brought very close to each other. Although from the existing information available with the author, and looking to the fact that the region to the S and E beyond the present study area is yet to be investigated, it is only possible to conclude that here the rocks show superimposition of a F_3 synform on the two limbs of a large F_2 fold.

6. Another important structural aspect which has emerged from this study is that in the study area, the degree of overturning increases from N to S. As is seen from the structural map (Fig. 4.1), there is presence of vertical axial plane fractures and foliations around Ditwas where the F_2 folds are almost upright. In the southern parts of the study area, the foliations get overturned as a result of which they dip gently towards the NW. This points to the possibility that during the D_2 deformation, a regional simple shear component was active along with the shortening (i.e. pure shear component). In other words the deformation must have occurred by non-ideal simple shear with both simple and pure shear components.

7. To develop F_1-F_2 folds with NE-SW trending axis, the shortening direction and the accompanying shear component active during D_1-D_2 deformation must have been NW-SE. There is presence of a strong NW-SE trending mineral lineation (stretching lineation) on the S_1-S_2 foliations in some parts of the study area lying to the S of Lunavada-Santrampur line. According to the author, this lineation

developed during the D_1-D_2 deformation due to shearing which is related to movement along foliations.